Macroscopic Quantum Behaviour

Superconductivity and Cold Atomic Gases

by

Thomas P. Davis

B.Sc., University of Guelph, 2000
M.Sc., University of British Columbia, 2002

A THESIS SUBMITTED IN PARTIAL FULFILMENT OF
THE REQUIREMENTS FOR THE DEGREE OF

Doctor of Philosophy

in

The Faculty of Graduate Studies

(Physics)

The University of British Columbia

July, 2006

Abstract

The study of physics at the atomic scale led to the development of quantum mechanics in the early twentieth century. Since then, quantum mechanics has developed into one of the most successfully tested of all physical theories.

Central to quantum mechanics is the concept of coherence. Keeping quantal coherence over large time scales or macroscopic length scales has proven to be a difficult, but fruitful endeavour both theoretically and experimentally. Two manifestations of this so-called macroscopic quantum coherence will be investigated in this thesis; the century-old field of superconductivity and the decade-old field of cold atomic gases.

Yttrium barium copper oxide is a layered superconductor whose transition temperature can be changed by controlling the amount of oxygen found between the copper oxide planes. Motivated by recent experiments where the penetration depth along the direction perpendicular to the copper oxygen planes was measured on extremely underdoped samples, a theoretical model is constructed which phenomenologically explains the observed electrodynamic properties.

The field of atomic physics underwent a revolution in 1994 when dilute atomic gases were cooled to nanokelvin temperatures, which resulted in the much sought after Bose-Einstein condensate. In the past decade, ultra-cold atomic experiments have been used to study fundamental quantum mechanics and more recently, with the application of optical lattices, many-body physics.

The second project contained in this thesis investigates a method to engineer the emergence of Dirac Fermions in an ultra-cold Fermionic gas with the application of an optical lattice. The Hamiltonian governing the low energy properties of this system is well known, and is shown to undergo a quantum phase transition where the low energy Fermionic quasiparticles acquire a mass, due to the appearance of "antiferromagnetic" ordering.

Contents

List of Figures

ACKNOWLEDGEMENTS

I would like to acknowledge the guidance and support of all of my teachers throughout my time in physics. Elisabeith Nicol, John Holbrook, Bernie Nickel, Chris Gray, Gordon Semenoff among many others, have all made an indelible impression on me and my work. I would like to acknowledge the effort my committee put into my PhD. Eric Zhitnisky, Doug Bonn and Ian Affleck were always available to lend their nearly infinite wisdom to bear on my project, and help me along the way. I would like to extend my deepest thanks to Kirk Madison, whose guidance and encouragement was crucial in devising, undertaking and completing the second half of this thesis.

This thesis would not exist without my supervisor Marcel Franz. I appreciate his unique style of doing physics, pursuing what is both interesting and relevant, and quickly apprehending what is germane, and what is superfluous, leading to quick insights into difficult problems. I found much solace in a piece of wisdom he passed on to me: "When you finish your bachelor's degree, you think you know everything. When you finish your master's degree you realize you know nothing. But when you finish your doctorate, you realize that it's OK since nobody else knows anything anyway."

I would like to acknowledge all the people who kept me sane throughout my years of graduate study. The guys: Phil Eles, Bojan Losic, Scott Noble and Inaki Olabarietta. My fellow condensed matter theorist, and person who helped me throughout grad school: Tami Pereg-Barnea. My office mates: Kirk Buckley, Greg Van Anders, Lara Thompson and Henry Ling. All of you have seriously impacted my education and I've ended up learning much outside of the narrow confines of physics.

My family has always been there to lend a supporting word. Mom, Dad, Leigh, Brent, thank you. My wife Heather Davis neé Nicholson. Always there to keep me on track, to debate the nature of academia versus the real world. To keep me down to earth and to continually challenge me. It is through our interactions that I've learned more about myself than I ever knew. I hope in the future we can continue to learn about each other, and never stop finding

new and interesting things to talk about.

I would like to thank all of the above for positively contributing to my work and my life. I would finally like to acknowledge that physics is hard.

CHAPTER 1

INTRODUCTION

At the end of the nineteenth century James Clerk Maxwell wrote down the equations that unified the physics of electricity and magnetism. In so doing, the edifice of classical physics was complete, but not without its mysteries. The application of classical ideas to the physics at atomic length scales proved inadequate.

This introductory chapter will succinctly describe classical mechanics, followed by P. A. M. Dirac's prescription to quantize simple mechanical systems. Subsequently, classical electrodynamics – the simplest of all field theories – will be described and quantized. Finally, the concept of coherence in quantum mechanics will be introduced.

1.1 CLASSICAL MECHANICS

Lagrange's formulation of classical mechanics concisely states that the time integral of the Lagrangian, defined as the difference of the kinetic and potential energies

$$L(x, \dot{x}) = T(\dot{x}) - U(x, \dot{x}), \tag{1.1}$$

achieves a minimum at the classical trajectory of the particle

$$\frac{\delta}{\delta x(t)} \int_{t_1}^{t_2} L(x(t), \dot{x}(t)) dt \Big|_{x(t)=x_{Cl}(t)} = 0. \tag{1.2}$$

This gives an expedient way of deriving the equations of motion,

$$\frac{\partial L(x, \dot{x})}{\partial x} - \frac{d}{dt} \frac{\partial L(x, \dot{x})}{\partial \dot{x}} = 0, \tag{1.3}$$

at the expense of physical intuition.

Hamilton derived an equivalent formulation by first defining the canonical momentum

$$p \equiv \frac{\partial L}{\partial \dot{x}} \tag{1.4}$$

and then considering the Legendre transformation of the Lagrangian,

$$H(p,x) = p\dot{x} - L(p,x), \tag{1.5}$$

now known as the Hamiltonian. The equations of motion are given by derivatives of the Hamiltonian

$$\dot{x} = \frac{\partial H(p,x)}{\partial p}, \tag{1.6}$$

and

$$\dot{p} = -\frac{\partial H(p,x)}{\partial x}. \tag{1.7}$$

Under most circumstances, the Hamiltonian is the total energy of the system. However, the Hamiltonian also plays another, more fundamental role. The time dependence of any quantity

$$\dot{\Omega}(p,x) = \frac{\partial \Omega(p,x)}{\partial x}\dot{x} + \frac{\partial \Omega(p,x)}{\partial p}\dot{p} \tag{1.8}$$

can be written in terms of the Hamiltonian

$$\dot{\Omega}(p,x) = \frac{\partial \Omega(p,x)}{\partial x}\frac{\partial H(p,x)}{\partial p} - \frac{\partial \Omega(p,x)}{\partial p}\frac{\partial H(p,x)}{\partial x} \tag{1.9}$$

by using the equations of motion 1.6 and 1.7. The above combination of partial derivatives occurs often enough in classical physics to warrant the notation

$$\{\Omega, \kappa\} \equiv \frac{\partial \Omega}{\partial x}\frac{\partial \kappa}{\partial p} - \frac{\partial \Omega}{\partial p}\frac{\partial \kappa}{\partial x} \tag{1.10}$$

and the name "Poisson bracket". Therefore, the time dependence of any quantity in classical physics is governed by the Hamiltonian via the Poisson bracket

$$\dot{\Omega}(p,x) = \{\Omega(p,x), H(p,x)\}. \tag{1.11}$$

Consequently, the classical conservation laws are obtained by finding quantities that have a vanishing Poisson bracket with the Hamiltonian.

The Poisson bracket plays a central role in Hamilton's formulation of classical mechanics by defining the concept of "canonical conjugation". Two variables are said to be "canonically conjugate" if their Poisson bracket is equal to one. For example, momentum, p, as defined in equation 1.4 is canonically conjugate to position, x, since

$$\{x, p\} = 1. \tag{1.12}$$

Furthermore, a "canonical transformation" is a transformation from one set of variables to another that preserve the Poisson brackets. Any set of variables that preserve the fundamental Poisson brackets can be used to solve the system. This usually allows for a great simplification of the Hamiltonian, but more importantly, it reveals that position and momentum are only a subset of possible "generalized coordinates" that can equally describe a given physical system.

1.2 Quantization of Classical Mechanics

The first task in quantizing a physical system is to augment the observables, such as position and momentum, to mathematical operators:

$$x \rightarrow \hat{x}, \tag{1.13}$$

$$p \rightarrow \hat{p}. \tag{1.14}$$

Secondly, the Poisson brackets are augmented to "canonical commutation relations" divided by the imaginary unit and a new fundamental constant of nature with dimensions of action, $\hbar$:

$$\{\Omega, \kappa\} \rightarrow \frac{1}{i\hbar}\left[\hat{\Omega}, \hat{\kappa}\right], \tag{1.15}$$

$$\equiv \frac{1}{i\hbar}\left(\hat{\Omega}\hat{\kappa} - \hat{\kappa}\hat{\Omega}\right). \tag{1.16}$$

This prescription to find the "quantum conditions" is due to Dirac. For example, the position momentum quantum condition is

$$[\hat{x}, \hat{p}] = i\hbar. \tag{1.17}$$

The quantum operators must now act on something, and that something is a fundamentally new object that does not appear in classical physics. "The states and dynamical variables have to be represented by mathematical quantities of different natures from those ordinarily used in physics."[4] The new object, called a 'state vector' $|\psi\rangle$, is mathematically described by a vector in Hilbert space, and contains all of the physical information about the system.

Observables in classical mechanics correspond to Hermitian operators in quantum mechanics, whose observable information is now obtained by a quantum 'averaging' over the state vector;

$$\Omega_{\text{Obs}} = \langle\psi|\hat{\Omega}|\psi\rangle. \tag{1.18}$$

Quantum averaged Hermitian operators become the classical dynamical variables in the so-called "classical limit" of $\hbar \to 0$.

The time evolution of any observable is obtained from the quantum prescription applied to equation 1.11:

$$\frac{\partial}{\partial t}\langle\psi|\hat{\Omega}|\psi\rangle = \frac{1}{i\hbar}\langle\psi|\left[\hat{\Omega}, \hat{H}\right]|\psi\rangle. \tag{1.19}$$

Assuming that there is no explicit time dependence of the operator $\hat{\Omega}$, and ascribing all of the time dependence to the state vector[1], leads to the equation that governs the time evolution of the state vector

$$i\hbar\frac{\partial}{\partial t}|\psi\rangle = \hat{H}|\psi\rangle, \tag{1.20}$$

known as the Schrödinger equation.

A general state vector can be constructed from any complete set of basis states $|i\rangle$ as

$$|\psi\rangle = \sum_i a_i|i\rangle, \tag{1.21}$$

or, if the basis states form a continuum,

$$|\psi\rangle = \int d\eta F(\eta)|\eta\rangle. \tag{1.22}$$

[1]This corresponds to the Schrödinger picture, as it was with this assumption that he first derived the wave mechanics.

The most useful bases are those that are formed from the eigenstates of physical operators. The 'position' basis is defined by the eigenvalues of the position operator

$$\hat{x}|x\rangle = x|x\rangle. \tag{1.23}$$

A general state in the position basis is written

$$|\psi\rangle = \int dx\psi(x)|x\rangle, \tag{1.24}$$

where the function $\psi(x)$, known as the 'wavefunction', gives the resolution of the state into each eigenstate of the position operator. The action of the position operator in the position basis is given trivially by equation 1.23, a simple multiplication by the coordinate:

$$\hat{x}\psi(x) = x\psi(x). \tag{1.25}$$

The action of the momentum operator needs to be chosen to satisfy the canonical commutation relations 1.17

$$\begin{aligned} [\hat{x},\hat{p}]\,\psi(x) &= i\hbar\psi(x), & (1.26)\\ &= \hat{x}\hat{p}\psi(x) - \hat{p}\hat{x}\psi(x). & (1.27) \end{aligned}$$

This simpler condition compels the identification of the momentum operator with differentiation with respect to position

$$\hat{p} = \frac{\hbar}{i}\frac{\partial}{\partial x} \tag{1.28}$$

in the position basis. Conversely, the position operator in the momentum basis is identified with differentiation with respect to momentum.

Knowledge of the wavefunction in one basis is sufficient to determine its form in any basis. All that is needed to transform between bases is the overlap between the basis vectors. For instance, to transform between the momentum and position representation, one needs the overlap $\langle p|x\rangle$, and the transformation is accomplished via

$$\psi(p) = \langle p|\psi\rangle = \int dx\psi(x)\langle p|x\rangle. \tag{1.29}$$

This is calculated by acting the momentum operator to the left and the right of the overlap

$$\langle p|\hat{p}|x\rangle = p\langle p|x\rangle, \tag{1.30}$$

$$\langle p|\hat{p}|x\rangle = \frac{\hbar}{i}\frac{\partial}{\partial x}\langle p|x\rangle. \tag{1.31}$$

Equating the two results in a differential equation with solution[2]

$$\langle p|x\rangle = \frac{1}{\sqrt{2\pi\hbar}}e^{\frac{i}{\hbar}px}. \tag{1.36}$$

Therefore, the position and momentum wavefunctions are related by Fourier transformation. This result holds generally for any canonically conjugate variables.

One consequence of the non-commutativity of operators is the Heisenberg uncertainty principle of quantum mechanics. There exists a fundamental limit to the precision that can be obtained when measuring the observables that correspond to two non-commuting quantum operators:

$$(\Delta\Omega\Delta\kappa)^2 \geq \frac{1}{4}\langle[\hat{\Omega},\hat{\kappa}]\rangle^2, \tag{1.37}$$

where $\Delta\Omega \equiv \sqrt{\langle\hat{\Omega}^2\rangle - \langle\hat{\Omega}\rangle^2}$. This principle reflects the fact that quantum mechanics reveals a physical distinction between large and small. A small system obeys quantum mechanics where the act of observation affects, and

[2]That the magnitude of the overlap is $\frac{1}{\sqrt{2\pi\hbar}}$ in one spatial dimension is shown by first noting that

$$\int dx|x\rangle\langle x| = 1 \tag{1.32}$$

and therefore

$$\langle p'|p\rangle = \int dx\langle p'|x\rangle\langle x|p\rangle \tag{1.33}$$

$$= \mathcal{N}^2\int dx \exp\left(\frac{i}{\hbar}(p-p')x\right) \tag{1.34}$$

$$= (\mathcal{N}^2 2\pi\hbar)\,\delta(p-p'). \tag{1.35}$$

cannot be disentangled from, the system under study. For example, position and momentum obey the uncertainty relation

$$\Delta x \Delta p \geq \frac{\hbar}{2}, \tag{1.38}$$

revealing that the order of observation is important, since the quantum operators do not commute.

Measurements in quantum mechanics affect the system by "collapsing" the system into an eigenstate of the corresponding Hermitian operator. For example, after a measurement of position, the quantum state will be in an eigenstate of the position operator, which corresponds to a completely uniform momentum state. Therefore a subsequent measurement of the momentum will reveal any value with equal likelihood.

1.3 Classical Electrodynamics

The Maxwell equations, alluded to earlier,

$$\vec{\nabla} \cdot \vec{E} = \rho, \tag{1.39}$$

$$\vec{\nabla} \times \vec{E} = -\frac{\partial \vec{B}}{\partial t}, \tag{1.40}$$

$$\vec{\nabla} \cdot \vec{B} = 0, \tag{1.41}$$

$$\vec{\nabla} \times \vec{B} = \frac{\partial \vec{E}}{\partial t} + \vec{j}, \tag{1.42}$$

contain the physics of classical electrodynamics[3].

Since the magnetic field is divergenceless by equation 1.41, it can be written as the curl of another vector

$$\vec{B} = \vec{\nabla} \times \vec{A} \tag{1.43}$$

the "vector potential". A rearrangement of 1.40

$$\vec{\nabla} \times \left\{ \vec{E} + \frac{\partial}{\partial t} \vec{A} \right\} = 0 \tag{1.44}$$

[3]The units chosen are "Heaviside-Lorentz rationalized units". For a discussion on the units used throughout this thesis, please consult Appendix B.

similarly admits a definition of the "scalar potential"

$$\vec{E} = -\vec{\nabla}\phi - \frac{\partial}{\partial t}\vec{A}, \tag{1.45}$$

resulting in the potential form of Maxwell's equations

$$\vec{\nabla}\left(\vec{\nabla}\cdot\vec{A}\right) - \nabla^2\vec{A} + \frac{\partial}{\partial t}\vec{\nabla}\phi + \frac{\partial^2}{\partial t^2}\vec{A} = \vec{j}, \tag{1.46}$$

$$-\nabla^2\phi - \frac{\partial}{\partial t}\vec{\nabla}\cdot\vec{A} = \rho. \tag{1.47}$$

By writing these equations in a symmetric form

$$\left(\frac{\partial^2}{\partial t^2} - \nabla^2\right)\vec{A} + \vec{\nabla}\left(\frac{\partial}{\partial t}\phi + \vec{\nabla}\cdot\vec{A}\right) = \vec{j} \tag{1.48}$$

$$\left(\frac{\partial^2}{\partial t^2} - \nabla^2\right)\phi - \frac{\partial}{\partial t}\left(\frac{\partial}{\partial t}\phi + \vec{\nabla}\cdot\vec{A}\right) = \rho \tag{1.49}$$

suggests the introduction of relativistic four vector notation[4]

$$\partial_\mu = \left(\frac{\partial}{\partial t}, -\vec{\nabla}\right), \tag{1.50}$$

$$A_\mu = \left(\phi, \vec{A}\right), \tag{1.51}$$

$$j_\mu = \left(\rho, \vec{j}\right), \tag{1.52}$$

as all of Maxwell's equations can be written in the concise form[5]

$$\partial^2 A_\nu - \partial_\nu\left(\partial_\mu A^\mu\right) = j_\nu. \tag{1.53}$$

1.4 Quantization of Electrodynamics

To quantize the theory of electrodynamics according to Dirac's prescription, a Lagrangian needs to be constructed. Since electrodynamics is a field theory

[4]Changing between covariant and contravariant vectors simply changes the sign of the spatial part of the four vector – the simple flat spacetime metric $g_{\mu\nu} = \mathrm{diag}(1, -1, -1, -1)$ will be used throughout this thesis.

[5]It is no surprise that Maxwell's equations have such an elegant form when written in relativistic notation; the theory of special relativity was originally derived from the assertion that the equations of electrodynamics are valid in all frames of reference.

with continuous variables, a Lagrangian density $\mathcal{L}$ is introduced, where

$$L = \int \mathrm{d}^3 x \mathcal{L}. \tag{1.54}$$

This necessitates the augmentation of the Euler-Lagrange equation 1.3 to

$$\frac{\partial \mathcal{L}}{\partial \eta} - \partial^\mu \frac{\partial \mathcal{L}}{\partial \left(\partial_\mu \eta\right)} = 0. \tag{1.55}$$

What Lagrangian density gives rise to Maxwell's equations? The source term can be easily handled by the Lagrangian

$$\mathcal{L}' = -j_\mu A^\mu \tag{1.56}$$

leading to the requirement

$$\partial^\mu \frac{\partial \mathcal{L}}{\partial \left(\partial_\mu A_\nu\right)} = \partial^\mu \left(\partial_\mu A_\nu - \partial_\nu A_\mu\right), \tag{1.57}$$

which requirement can be satisfied by setting

$$\mathcal{L} = \partial^\mu A^\nu \left(\partial_\mu A_\nu - \partial_\nu A_\mu\right) \tag{1.58}$$

however this is not quite right. The reason is that there is a redundancy in the definitions of the potentials. Looking back to equations 1.43 and equation 1.45, the potentials can be changed by and arbitrary function

$$A'_\mu = A_\mu - \partial_\mu \chi \tag{1.59}$$

without affecting the physical electromagnetic fields. This transformation 1.59 is known as a gauge transformation, and Maxwell's equations written in potential form are gauge invariant. Therefore, the Lagrangian must also be gauge invariant. To retain gauge invariance, the Lagrangian 1.58 is symmetrized with respect to $\mu \leftrightarrow \nu$, giving the correct electrodynamic Lagrangian

$$\mathcal{L} = -\frac{1}{4} F^{\mu\nu} F_{\mu\nu} - j_\mu A^\mu, \tag{1.60}$$

where the electromagnetic field strength tensor

$$F_{\mu\nu} = \partial_\mu A_\nu - \partial_\nu A_\nu \tag{1.61}$$

has been introduced. This tensor is the generalization of the curl operator to four dimensions and is manifestly gauge invariant. Furthermore, the elements $-F_{0i}$ give the i^{th} components electric field and $-\epsilon_{ijk}F_{ij}$ give the k^{th} components of the magnetic field. The Lagrangian, which is the trace of the square of the field tensor, written in terms of the electric and magnetic fields is given by the expression

$$\mathcal{L} = -\frac{1}{2}\left(E^2 - B^2\right) + \rho\phi - \vec{j}\cdot\vec{A}. \tag{1.62}$$

The next step in quantizing electrodynamics is to construct the canonical momentum density

$$\pi_\mu = \frac{\partial\mathcal{L}}{\partial\dot{A}_\mu} = \partial_0 A_\mu - \partial_\mu A_0, \tag{1.63}$$

and the Hamiltonian[6]

$$H = \sum_i p_i\dot{x}_i - L + \int \mathrm{d}^3x \left\{\pi_\mu\dot{A}_\mu - \mathcal{L}\right\}. \tag{1.64}$$

The spatial components of the canonical electromagnetic momentum density are the components of the electric field. The temporal component, however, vanishes. This is the first indication that Dirac's canonical quantization will not be sufficient to quantize relativistic electrodynamics. At the heart of its failure is the symmetry of spatial and temporal coordinates dictated by relativistic invariance. Hamiltonian dynamics, and therefore canonical quantization, treats the temporal direction differently from spatial directions.

There are two ways to proceed. The method that preserves the full relativistic invariance of the theory treats the condition $\pi_0 = 0$ as a constraint, augment the Poisson brackets to "Dirac" brackets and quantize from there[4]. However, for the purposes of this thesis, it is not necessary to keep the full relativistic invariance of electrodynamics. A specific gauge is adopted, where[7]

$$\vec{\nabla}\cdot\vec{A} = 0, \tag{1.65}$$

[6]Specifically, this is the free particle Hamiltonian coupled to electrodynamics.

[7]This gauge is known by a number of names, such as "radiation" gauge, "physical" gauge and most commonly "Coulomb" gauge.

and the two Maxwell equations become

$$\partial^2 \vec{A} + \frac{\partial}{\partial t}\vec{\nabla}\phi = \vec{j}, \tag{1.66}$$

$$-\nabla^2 \phi = \rho. \tag{1.67}$$

At this point, the two Maxwell equations look to be dependent. However, recalling the Helmholtz decomposition of a vector into transverse and longitudinal components

$$\vec{X} = \vec{X}_T + \vec{X}_L, \tag{1.68}$$

where

$$\vec{\nabla} \cdot \vec{X}_T = 0, \tag{1.69}$$

$$\vec{\nabla} \times \vec{X}_L = 0. \tag{1.70}$$

reveals that, in the Coulomb gauge, the vector potential is completely transverse. Therefore analyzing the longitudinal part of equation 1.66 reveals

$$\frac{\partial}{\partial t}\nabla^2 \phi = \vec{\nabla} \cdot \vec{j}_L \tag{1.71}$$

and in conjunction with the other Maxwell equation can be rewritten

$$\partial_\mu j_L^\mu = 0, \tag{1.72}$$

which is nothing other than the conservation of local electrical charge, and connects the longitudinal part of the current with moving physical charges.

The transverse part of 1.66 gives the wave equation

$$\partial^2 \vec{A} = \vec{j}_T \tag{1.73}$$

whose source-free solutions are plane waves with characteristic velocity c, and dispersion $\omega = ck$.

The classical Hamiltonian that governs electrodynamics in the Coulomb gauge can be constructed

$$H = \frac{\left(\vec{p} - e\vec{A}\right)^2}{2m} + \frac{1}{2}\int \mathrm{d}^3x \left(E^2 + B^2\right), \tag{1.74}$$

and is the starting point for the non-relativistic quantization of electrodynamics, in accordance with Dirac's prescription.

The canonical commutation relation

$$[A_i(x,t), \pi_j(y,t)] = i\hbar\delta_{ij}\delta(x-y), \tag{1.75}$$

can be satisfied by the solution of the source-free Maxwell equation 1.66

$$\vec{A}(x,t) = \sum_{k\lambda} \hat{e}_{k\lambda} \left(A_{k\lambda} e^{i(kx-\omega t)} + A^{\dagger}_{k\lambda} e^{-i(kx-\omega t)} \right) \tag{1.76}$$

with the introduction of the operators

$$a_{k\lambda} = \sqrt{\frac{\hbar\omega_k}{2}} A_{k\lambda}, \tag{1.77}$$

$$a^{\dagger}_{k,\lambda} = \sqrt{\frac{\hbar\omega_k}{2}} A^{\dagger}_{k\lambda} \tag{1.78}$$

subject to the conditions

$$[a_{k\lambda}, a_{k'\lambda'}] = [a^{\dagger}_{k\lambda}, a^{\dagger}_{k'\lambda'}] = 0, \tag{1.79}$$

and

$$[a_{k\lambda}, a^{\dagger}_{k'\lambda'}] = \delta_{kk'}\delta_{\lambda\lambda'}. \tag{1.80}$$

Expanding the electromagnetic part of the Hamiltonian 1.74 in terms of the potentials[8]

$$H_{EM} = \frac{1}{2}\int \mathrm{d}^3x \left(\dot{\vec{A}}^2 + (\vec{\nabla}\times\vec{A})^2 \right) + \int \mathrm{d}^3x \mathrm{d}^3y \frac{\rho(x)\rho(y)}{|x-y|} \tag{1.81}$$

The Hamiltonian is quadratic in terms of the operators 1.77 and 1.78

$$H_{EM} = \sum_{k\lambda} \hbar\omega_k a^{\dagger}_{k\lambda} a_{k\lambda} + E_0. \tag{1.82}$$

[8]The cross term proportional to $\vec{\nabla}\phi \cdot \vec{A}$ vanishes in the Coulomb gauge after an integration by parts, and the second cross term proportional to $(\nabla\phi)^2$ is rewritten as the Coulombic term in equation 1.81 after an integration by parts, and invoking the general solution to Laplace's equation 1.67.

The problem of quantization of electrodynamics in the Coulomb gauge is now reduced to finding the spectrum of the operator $a^\dagger a$ for each mode in the electromagnetic cavity.

Given the eigenvalue equation

$$a^\dagger a|\psi_n\rangle = \epsilon_n|\psi_n\rangle \tag{1.83}$$

the eigenvalues of the states $a|\psi_n\rangle$ and $a^\dagger|\psi_n\rangle$ are found using the commutation relation $[a, a^\dagger] = 1$ to be

$$a^\dagger a\left(a|\psi_n\rangle\right) = (\epsilon_n - 1)a|\psi_n\rangle \tag{1.84}$$
$$a^\dagger a\left(a^\dagger|\psi_n\rangle\right) = (\epsilon_n + 1)a^\dagger|\psi_n\rangle \tag{1.85}$$

The eigenstates of $a^\dagger a$ are strictly positive, since

$$\langle\psi_n|a^\dagger a|\psi_n\rangle = |a|\psi_n\rangle|^2 \geq 0. \tag{1.86}$$

Therefore, there exists a state with zero eigenvalue. These two pieces of information together give the whole spectrum of $a^\dagger a$, which consists of states labeled by the natural numbers

$$|\psi_n\rangle = \{|n\rangle; n \in \mathbb{Z}\}, \tag{1.87}$$

with integer eigenvalues

$$a^\dagger a|n\rangle = n|n\rangle. \tag{1.88}$$

Therefore, the spectrum of the quantized electromagnetic Hamiltonian[9]

$$H_{EM} = \sum_{k\lambda} a^\dagger_{k\lambda} a_{k\lambda} \tag{1.89}$$

can be labeled by the number of excitations in each mode of the electromagnetic cavity $|n_{k1\lambda}, n_{k2\lambda}\cdots\rangle$ with energy

$$E = \hbar \sum_{k\lambda} k n_{k\lambda}. \tag{1.90}$$

[9]The constant (infinite) energy E_0 is omitted, since for condensed matter and atomic physics applications, it will not affect the outcome of experiments.

1.5 Coherence in Quantum Mechanics

Just as the momentum and position operators have eigenstates

$$\hat{x}|x\rangle = x|x\rangle, \tag{1.91}$$
$$\hat{p}|p\rangle = p|p\rangle, \tag{1.92}$$

so too does the lowering operator a. The action of this operator on a general state written in the number basis

$$a|z\rangle = \mathcal{N}\sum_{n=0}^{\infty} g_n a|n\rangle \tag{1.93}$$
$$= \mathcal{N}\sum_{n=0}^{\infty} g_{n+1}\sqrt{n}|n\rangle \tag{1.94}$$

gives a recursion relation

$$g_{n+1} = \frac{z}{\sqrt{n}} g_n \tag{1.95}$$

whose solution gives the normalized eigenstate

$$|z\rangle = e^{-\frac{1}{2}|z|^2}\sum_{n=0}^{\infty}\frac{z^n}{n!}|0\rangle. \tag{1.96}$$

The eigenstates of the lowering operator a form an over-complete set labeled by the complex parameter z. Writing z in polar form, the state 1.96 becomes

$$|z\rangle = e^{-\frac{1}{2}|z|^2}\sum_{n=0}^{\infty} e^{in\theta}\frac{|z|^n}{\sqrt{n!}}|n\rangle. \tag{1.97}$$

The operation of differentiation with respect to θ has the same effect as the number operator on the state 1.97. This suggests the conjugate relationship between phase and particle number

$$[\hat{n}, \hat{\theta}] = i, \tag{1.98}$$

which can be strictly proven[10].

[10]In fact, this equation is not completely correct. The true relation is

$$\left[\hat{n}, \hat{\theta}\right] = i\left(1 - 2\pi\delta_{2\pi}(\theta)\right), \tag{1.99}$$

This relationship, according to equation 1.37, immediately implies that there is an uncertainty relation between particle number and quantal phase. States with a definite number of particles, so-called Fock states, therefore have a completely uncertain phase. Conversely, states with a definite quantal phase have a completely uncertain number of particles, such as the eigenstates 1.96 which are known as "coherent states".

Coherent states were first introduced in 1963 by R. J. Glauber[11][6] who showed that the coherent states of the electomagnetic field best approximate classical solutions to Maxwell's equations. A laser generates a single coherent state, while incoherent sources are described by a statistical mixture of coherent states.

The complex macroscopic wavefunction,

$$\phi(x) = \langle x|z\rangle, \tag{1.101}$$

is a quantum mechanical wavefunction that describes a macroscopic collection of particles. The complex phase associated with this wavefunction when written in polar coordinates

$$\phi(x) = |\phi(x)|e^{i\theta(x)} \tag{1.102}$$

is identified with the quantal phase. Is it reasonable to ascribe a physical significance to quantal phase?

Since particle number is generally a conserved quantity, it may seem reasonable that quantal phase may not be a measurable (and therefore physical) quantity. However, a calculation of the particle number fluctuations in the state 1.96 reveals

$$\frac{\Delta n}{\langle n\rangle} = \frac{\sqrt{\langle n^2\rangle - \langle n\rangle^2}}{\langle n\rangle}, \tag{1.103}$$

$$= \frac{1}{|z|} = \frac{1}{\sqrt{\langle n\rangle}}, \tag{1.104}$$

where

$$\delta_{2\pi}(\theta) = \sum_{p=-\infty}^{\infty} \delta(\theta - 2p\pi), \tag{1.100}$$

the Dirac delta function restricted to the range $\{0, 2\pi\}$. For an excellent introduction and review of this intricate subject, see [5].

[11] Glauber was one of the three recipients of the Nobel prize in 2005.

implying that a state with a macroscopic occupation $\langle n \rangle \gg 1$ can have a definite quantal phase, while still preserving particle number to a good approximation. It is therefore reasonable that this quantal phase can be physically measured[12].

The remainder of this thesis is based on two different physical systems that manifest a macroscopic wavefunction. The first system studied is high temperature superconductors, where the macroscopic wavefunction describes paired electrons and therefore admits resistanceless electronic flow – perfect conductivity. Motivated by recent experiments on so-called "c-axis" electronic transport, a model is developed and successfully fit to the experimental data, constraining the ultimate theory of high T_C superconductors.

Secondly, the phenomenon of Bose-Einstein condensation is described, and a method of engineering an interesting quantum field theory is presented. Dirac Fermions arise in many condensed matter systems, as well as in particle physics. It is shown that they can be created in a suitably chosen optical lattice symmetry, whose perfect periodicity and tunable interaction parameters make this an ideal experiment to map out the phase diagram of interacting Dirac Fermions. A phase transition from a massless to a massive phase is predicted at a critical interaction parameter whose signature should be observable in the correlations of the density images obtained from different experimental images.

[12]Of course, the quantal phase cannot be measured in an *absolute* sense. It is only phase differences between two systems with macroscopic occupation, such as a Josephson junctions or the interference of two Bose condensates. The problem lies in the inability to create a universal phase standard to serve as the basis to measure all quantal phases. This point is discussed nicely in [7].

Chapter 2

Superconductivity as a Macroscopic Quantal Effect

The appearance of quantum coherence is a result of the macroscopic occupation of a single quantum state. A remarkable effect occurs when these particles are charged.

2.1 Introduction to Superconductivity

The first term in the Hamiltonian

$$H = \frac{(\vec{p} - e\vec{A})^2}{2m} + \sum_{k\lambda} \omega_k n_{k\lambda} + \int \mathrm{d}^3x \mathrm{d}^3y \frac{\rho(x)\rho(y)}{|x-y|}, \tag{2.1}$$

derived in the last chapter, describes the interaction between a charged particle and the electromagnetic field. The effect of the electromagnetic field on a quantum wavefunction can be found from the resulting Schrödinger equation

$$i\frac{\partial}{\partial t}\psi(x) = H\left(-i\nabla - eA, x\right)\psi(x). \tag{2.2}$$

A density current, which, for a charged system, is an electrical current, can be derived from equation 2.2 by finding the time derivative of the particle density

$$\frac{d|\psi|^2}{dt} = \frac{d\psi}{dt}\psi^* + \psi\frac{d\psi^*}{dt}, \tag{2.3}$$

which, by continuity (a manifestation of local particle number conservation), must be equal to the divergence of a current

$$\frac{d|\psi|^2}{dt} = -\vec{\nabla}\cdot\vec{j}. \tag{2.4}$$

The resulting current

$$\vec{j} = \frac{i}{2m}\left\{\left(\vec{\nabla}\psi\right)\psi^* - \psi\left(\vec{\nabla}\psi^*\right)\right\} - \frac{e}{m}\vec{A}|\psi|^2 \tag{2.5}$$

written in polar form

$$\vec{j} = \frac{1}{m}\left(\vec{\nabla}\theta - e\vec{A}\right)|\psi|^2 \tag{2.6}$$

admits a nonzero current, even when the particle density is constant in time; given that the quantal phase satisfies Laplace's equation and the particle density is constant in space.

In a typical geometry under these conditions, equation 2.6 becomes

$$\vec{j} = -\frac{e}{m}|\psi|^2\vec{A} \tag{2.7}$$

known as "London's equation"[8].

The consequences of London's equation are remarkable. First, by the strict definition of conductivity

$$\sigma_{ij} \equiv \frac{j_i}{E_j} \tag{2.8}$$

London's equation implies infinite conductivity, as there can be finite current with no electric field.

Secondly, by applying Maxwell's equation 1.40 to London's equation, the resulting equation

$$\nabla^2\vec{B} = -\lambda^2\vec{B}, \tag{2.9}$$

where $\lambda^2 = \frac{e|\psi|^2}{m}$, implies that no magnetic field can be present inside a region containing a charged macroscopic quantal system[1].

[1]The original justification of London's equation stemmed from classical considerations of electrons flowing in a material with no collisional resistance. This method arrives at a somewhat different version of London's equation, one for a 'perfect' conductor – a conductor that resists all change to the magnetic field in its interior. If a magnetic field is penetrating a material that becomes a perfect conductor, that magnetic field will be trapped in the material indefinitely. A superconductor, on the other hand, obeys London's equation 2.7 and will therefore expel all magnetic fields from its interior, regardless of history.

In 1911, exactly such a system was discovered by H. Kammerlingh Onnes, the first person to liquefy helium in his laboratory in Leiden, Netherlands. He noticed that elemental mercury lost all of its electrical resistance when cooled below $4.2K$. He labeled this new state of matter a 'superconductor', and his initial discovery would result in the first of five Nobel prizes awarded for the study of superconductivity[2].

Could this amazing new discovery be a manifestation of macroscopic quantum behaviour? Could this newly found superconductivity be a macroscopic occupation of electrons into one single state? While a tantalizing and promising possibility, the laws of quantum mechanics explicitly forbid this. The Pauli exclusion principle, together with the spin-statistics connection, indicates that the wavefunction describing particles with integer spin, known as "Bosons", must be symmetric under the interchange of any two particle:

$$|\psi_B(1;2)\rangle = +|\psi_B(2;1)\rangle \tag{2.10}$$

and the wavefunction describing particles with half-integer spins, known as "Fermions", must be anti-symmetric under the interchange of any two of the particles:

$$|\psi_F(1;2)\rangle = -|\psi_F(2;1)\rangle. \tag{2.11}$$

Since electrons are Fermions, the exclusion principle forbids two electrons from occupying the same quantum state, as the two-body wavefunction will vanish by symmetry. Therefore, superconductivity cannot be simply described by a macroscopic occupation of electrons in a single quantum state. The ingenious mechanism that overcame this mystery led to the theoretical description of superconductivity, and the second Nobel prize awarded in the field.

2.2 Conventional Superconductivity

In 1957 three physicists – Bardeen, Cooper and Schreiffer – published the monumental paper describing the mechanism of superconductivity[9]. The genesis of the theory was a variational calculation performed by Leon Cooper

[2]1913 - H. K. Onnes, 1972 - J. Bardeen, L. Cooper and R. Schreiffer, 1973 - L. Esaki, I. Gaiever and B. D. Josephson, 1987 - J. G. Bednorz and K. A. Mueller, and 2003 - A. A. Abrikosov, V. L. Ginzburg and A. J. Legget

proving that when two electrons with a net mutual attraction are added to the Fermi sea, the overall free energy is minimized when the two electrons form a correlated pair. John Bardeen showed that the overscreened interaction between quantized crystal vibrations, phonons, and electrons could, at low enough temperatures, overcome the Coulomb repulsion between the electrons to produce the required attractive interaction. The overall macroscopic many-body wavefunction, the BCS wavefunction, proposed by Bob Schreiffer, has a macroscopic number of electrons near the Fermi surface paired, with the exclusion principle overcome by the fact that the composite pairs have integer spin.

The reduced BCS Hamiltonian[3]

$$H = \sum_{p\sigma} (\epsilon(p) - \mu)\, c^\dagger_{p\sigma} c_{p\sigma} + \frac{1}{2} \sum_{pp'k\sigma\sigma'} g(p-p') c^\dagger_{p\sigma} c^\dagger_{p'\sigma'} c_{p+k\sigma'} c_{p'-k\sigma} \qquad (2.12)$$

is a deceptively simple Hamiltonian that contains enough physics to describe superconductivity. Bardeen, Cooper and Schreiffer used a well known technique known as mean-field theory to solve this Hamiltonian. The basic premise is to decouple the four Fermi term into a series of two Fermi terms interacting with a field representing the average (or 'mean') of the other two terms. Schematically:

$$\begin{aligned} c^\dagger_1 c^\dagger_2 c_3 c_4 \;\rightarrow\; & \langle c^\dagger_1 c_4\rangle c^\dagger_2 c_3 - \langle c^\dagger_1 c_3\rangle c^\dagger_2 c_4 + \langle c^\dagger_2 c_3\rangle c^\dagger_1 c_4 - \langle c^\dagger_2 c_4\rangle c^\dagger_1 c_3 \\ & + \langle c^\dagger_1 c^\dagger_2\rangle c_3 c_4 + \langle c_3 c_4\rangle c^\dagger_1 c^\dagger_2. \end{aligned} \qquad (2.13)$$

The first four terms simply renormalize the energy and chemical potential terms in the Hamiltonian and the last two give rise to terms with two creation or destruction operators, which, in a normal system, are identically zero. However, in a system with a macroscopic occupation, and therefore an uncertain number of particles, these 'anomalous' pairings give rise to bona fide terms in the Hamiltonian.

According to the BCS theory, the electron-phonon coupling produces an interaction that is isotropic in momentum space and attractive when the electron energies are sufficiently close to the Fermi energy. With these re-

[3]For the remainder of this thesis, the second quantized formalism will be used. For an excellent reference, see [10].

strictions, the mean-field reduced BCS Hamiltonian is

$$H = \sum_{p\sigma} \epsilon(p) c^{\dagger}_{p\sigma} c_{p\sigma} + \frac{g}{2} \sum_{pp'}^{|\epsilon|<\omega_D} \left\{ \langle c_{-p\downarrow} c_{p\uparrow} \rangle c^{\dagger}_{p'\uparrow} c^{\dagger}_{-p'\downarrow} + \langle c^{\dagger}_{p\uparrow} c^{\dagger}_{-p\downarrow} \rangle c_{-p'\uparrow} c_{p'\downarrow} \right\}, \tag{2.14}$$

where the energy is understood to be relative to the Fermi surface. Two improvements in notation greatly simplify this Hamiltonian. Introducing the mean field

$$\Delta = \frac{g}{2} \sum_{p}^{|\epsilon(p)|<\omega_D} \langle c_{-p\downarrow} c_{p\uparrow} \rangle \tag{2.15}$$

and the Nambu spinor

$$\psi_p = \begin{pmatrix} c_{p\uparrow} \\ c^{\dagger}_{-p\downarrow} \end{pmatrix}, \tag{2.16}$$

the Hamiltonian can be written in a very simple and compact form [4]

$$H = \sum_{p} \psi^{\dagger}_{p} \left[\epsilon(p)\sigma_3 + \Delta\sigma_1 \right] \psi_p, \tag{2.18}$$

from which the matrix valued Green's function can be read directly

$$\mathcal{G}(p,\omega) = \frac{\mathbb{1}w + \sigma_3\epsilon(p) + \sigma_1\Delta}{\omega^2 - \epsilon^2(p) - \Delta^2}. \tag{2.19}$$

The parameter Δ in equation 2.15 can now be calculated from the definition of the Green's function

$$\Delta = \frac{g}{4} \sum_{p}^{|\epsilon(p)|<\omega_D} \int_{-\infty}^{\infty} \frac{\mathrm{d}\omega}{2\pi} \mathrm{Tr}\mathcal{G}(p,\omega)\sigma_1, \tag{2.20}$$

[4] The conventional form of the Pauli matrices is adopted

$$\sigma_1 = \begin{pmatrix} 0 & 1 \\ 1 & 0 \end{pmatrix}, \sigma_2 = \begin{pmatrix} 0 & -i \\ i & 0 \end{pmatrix}, \sigma_3 = \begin{pmatrix} 1 & 0 \\ 0 & -1 \end{pmatrix}. \tag{2.17}$$

which leads to the self consistent equation

$$\frac{1}{D(\epsilon_F)g} = \int_0^{\omega_D} \mathrm{d}\epsilon \frac{1}{\epsilon^2 + \Delta^2} \tag{2.21}$$

known as the BCS gap equation. The solution of this equation

$$\Delta = \omega_D \sinh \frac{1}{D(\epsilon_F)g} \tag{2.22}$$

gives the numerical value of the mean field defined by equation 2.15, where $D(\epsilon_F)$ is the normal state density of states at the Fermi surface. This mean field has a number of interpretations: a thermodynamical order parameter whose non-zero value signals the breaking of local gauge invariance; an energy gap, since the modified energy spectrum

$$E(p) = \sqrt{\epsilon^2(p) + \Delta^2} \tag{2.23}$$

possesses a lower bound; and finally the macroscopic wavefunction that determines the behaviour of a macroscopic number of electrons near the Fermi surface.

At finite temperatures, the value of the gap is reduced. At the transition temperature T_c, the value of the gap reaches zero and superconductivity is destroyed.

To calculate temperature dependent quantities, the Matsubara formalism is used, which uses a correspondence between imaginary time and temperature to perform both quantum and thermodynamical averaging simultaneously [11]. Upon analytic continuation the imaginary time τ becomes a periodic variable with period β, the inverse temperature. Consequently, the Fourier transform is found in terms of discrete frequencies, the so-called Matsubara frequencies $i\omega_n$. The main calculational advantage in this formalism is that quantum and thermal averaging are easily performed by summation over the Matsubara frequencies. For a thorough introduction, consult [10].

The Matsubara Green's function for superconductivity is

$$\mathcal{G}(p, i\omega_n) = -\frac{\mathbb{1}(i\omega_n) + \epsilon(p)\sigma_3 + \Delta\sigma_1}{\omega_n^2 + \epsilon^2(p) + \Delta^2} \tag{2.24}$$

and the temperature dependent self consistent gap equation becomes

$$\Delta(T) = \frac{g}{4} \sum_p^{|\epsilon(p)|<\omega_D} \frac{1}{\beta} \sum_n \mathrm{Tr}\mathcal{G}(p, i\omega_n)\sigma_1, \tag{2.25}$$

whose solution when $\Delta \to 0$ is[5]

$$T_c = \frac{2e^{\gamma}}{\pi}\omega_D e^{-\frac{1}{\rho g}}. \tag{2.26}$$

When compared to the weak coupling solution of equation 2.22, the BCS ratio

$$\frac{\Delta}{T_c} = \frac{\pi}{e^{\gamma}} \approx 1.76 \tag{2.27}$$

is found. This value is seen in many elemental superconductors, establishing the BCS theory as the correct description of simple, weakly coupled superconductors.

2.3 High Temperature Superconductivity

A major goal of the superconductivity community was to produce materials with the highest transition temperature possible. It was thought that T_c's could not exceed 30K until 1986, when Bednorz and Mueller found a material with a T_c of 35K. A year later, the liquid nitrogen barrier had been broken with a compound whose T_c was 90K. These "high temperature" superconductors all have one feature in common: the existence of copper and oxygen forming two dimensional layered planes. Still considered to be the 'seat' of superconductivity, these copper oxygen planes have been central to most theories attempting to describe high T_c materials. The family of the high temperature superconductors containing lanthanum strontium copper oxide, yttrium barium copper oxide and calcium cobalt copper oxide, are amongst the family known as the cuprates. It is still the major goal of the superconductivity community to solve the mystery that surrounds the superconducting properties of the cuprates.

It was suspected by many very early that the description of the cuprates was to be found outside of the standard BCS theory. The symmetry of the pairing interaction was shown to be anisotropic[12, 13], and underdoped[6] cuprates were found to have a gap to transition temperature ratio much higher than the predicted BCS value of 1.76 (equation 2.27).

[5]Where $\gamma = \lim_{n\to\infty}\left(\sum_{k=1}^{n}\frac{1}{k} - \ln n\right) = 0.577215...$ is the Euler-Mascheroni constant.

[6]The transition temperature T_c of the cuprates can be continuously changed by chemically altering the amount of oxygen residing between the copper oxygen planes in a process known as doping.

Even though the underlying theory of the cuprates has yet to be determined, a phenomenologically successful Hamiltonian is found by imbuing a momentum dependence on the gap function

$$H = \sum_p \psi_p^\dagger \left[\epsilon(p)\sigma_3 + \Delta(p)\sigma_1\right] \psi_p, \tag{2.28}$$

which has been found to have d-wave[7] symmetry

$$\Delta(p) = \Delta_0 a^2 \left(p_x^2 - p_y^2\right) \tag{2.29}$$

$$= \Delta_0 \cos\left(2\phi\right) \tag{2.30}$$

in the cuprates (where a is some characteristic length within the system; the lattice parameter for example). This symmetry was deduced from a number of experiments, including careful penetration depths on pure crystals of YBCO, Josephson measurements that are sensitive to the phase of the order parameter and most conclusively the spontaneous generation of a flux quantum in a three-fold symmetric arrangement of crystals[13].

Beyond the symmetry of the order parameter, not much more is agreed upon in the cuprates. The central mystery is the so-called "mechanism" – the underlying physical process that mediates the electron-electron attraction akin to phonons in conventional superconductivity.

The cuprates are generally composed of insulating perovskites[8] whose transition temperature can be controlled by chemical substitution. This process, known as doping, removes a number of electrons on each copper oxygen plane. The undoped, or parent, compounds are insulators, which have exactly one conduction electron per copper atom, arranged antiferromagnetically and strong electron-electron repulsion forbids electron transport.

The magnetic order present in the parent compound quickly vanishes in YBCO with a small amount of oxygen doping. As doping is increased, the sample becomes superconducting. The transition temperature initially increases with further doping before attaining a maximum at "optimal doping", whereupon further doping decreases the transition temperature. This

[7]This nomenclature is borrowed from spectroscopy and the quantum orbitals of the hydrogen atom. Mathematically, it represents the symmetry of the dominant spherical harmonic in the expansion of $g(p-p')$ in the Hamiltonian 2.12.

[8]A perovskite is a technical name for the mineral titanium calcium oxide $CaTiO_3$, and is named after the Russian minearologist L .A. Perovski. It is now used for all compounds with the same general structure ABO_3.

information is usually summarized in a doping-temperature phase diagram, with doping increasing to the right. Compounds to the right of optimal doping are called "overdoped" and compounds to the left are called "underdoped". This information is typically displayed in a phase diagram, figure 2.1, where chemical doping is the abscissa and temperature the ordinate. However, the low temperature behaviour near the underdoped edge of the superconducting dome is the subject of recent debate and controversy, and the next chapter will endevour to shed light on this particular area of the phase diagram.

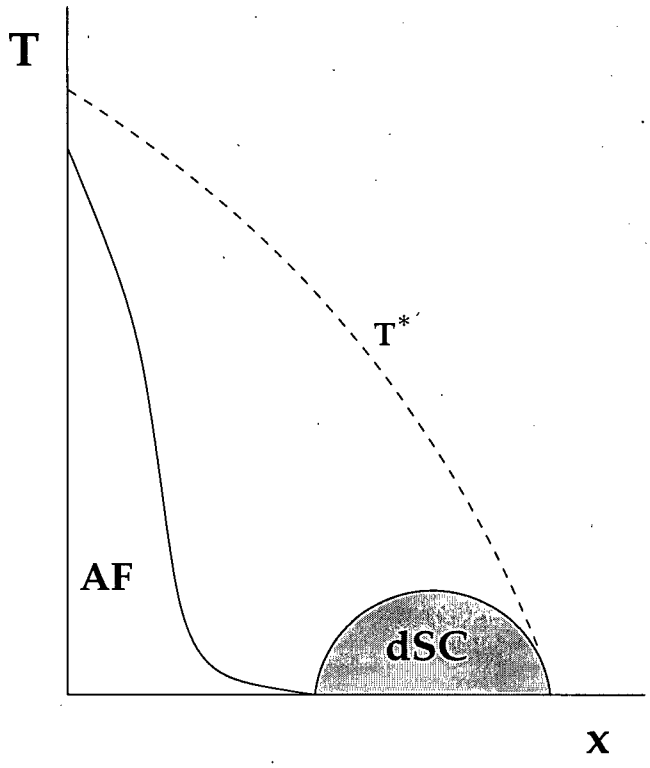

Figure 2.1: Canonical phase diagram for the cuprate superconductors. Chemical doping is the abscissa and temperature the ordinate. At zero doping the parent compounds are Mott insulators, where electron transport is forbidden due to strong electronic interactions, with antiferromagnetic Néel order. Upon chemical doping, this magnetic order is quickly destroyed and eventually superconductivity results. The next chapter of this thesis will focus on the extremely underdoped superconducting compounds, in order to shed light on a poorly understood region of the phase diagram.

CHAPTER 3

SUPERFLUID DENSITY

The electrodynamic response of a superconductor is governed by the electrons in the macroscopically occupied quantum state. This quantity, known as the superfluid density, has been the subject of intense study – both theoretically and experimentally.

In conventional s-wave superconductors, the low temperature superfluid density displays exponentially activated behaviour, as thermal excitations in a gapped system will display a Boltzmann distribution, with a strong insensitivity to material disorder. The early measurements on the cuprate superfluid density, on the other hand, displayed a non-exponential behaviour, implying a non-uniform gap function. The exact nature of this gap was the subject of a long debate. The experimental pursuit that eventually ended this debate rapidly drove the field of crystal growing resulting in the creation of extremely pure cuprate samples. Penetration depth measurements on these samples revealed the extrinsic effects of disorder were to mask the true, linear temperature dependence of the superfluid density – a clear hallmark of a d-wave order parameter.

Subsequently, a plethora of data was generated confirming the d-wave symmetry of the cuprate order parameter. This specific symmetry dictates a sign change in the order parameter upon a rotation of $\pi/2$, which was exploited in a number of phase sensitive experiments[13].

It became generally accepted that the BCS theory was the correct description of the overdoped cuprate superconductors. Flux quantization showed that Cooper pairs exist with charge $2e$ and the BCS gap ratio was the correct order of magnitude. However, below optimal doping, the BCS picture started to fail. Most notably, the magnitude of the gap maximum continued to increase[1], while T_c plummeted, in stark violation of the BCS gap ratio. Furthermore, the "normal" state is far from normal, displaying a non-Fermi

[1]This statement assumes that the depression in the density of states above T_C in the cuprates is due to incipient superconductivity, and therefore this "pseudogap" is the relevant parameter to use when calculating the BCS gap ratio. This is still controversial.

liquid resistivity curve, and a suppression in the density of states above T_c.

The difficult theoretical problem posed by the cuprates is thought to be related to the open theoretical question of doping a Mott insulator[14]. Therefore, experiments performed at the lowest superconducting doping levels will provide crucial information towards the resolution of this fundamental challenge.

Historically, experiments revealing the temperature dependent superfluid density gave some of the most compelling evidence for the unconventional nature of the cuprate superconductors. It was empirically determined that

$$\rho_s^{ab}(T) \approx ax - bT. \tag{3.1}$$

The linear temperature dependence arises simply within the BCS theory with an unconventional d-wave symmetry of the order parameter. The doping dependence, however, is mysterious, and difficult to reconcile within the BCS framework. Much of the theoretical effort has been devoted to replacing the BCS paradigm, and some (such as the resonance valence bond [15] and Gutzwiller projection techniques[16]) have even successfully predicted the linear doping dependence. However, these methods generally predict a strong doping dependence of the coefficient in front of the temperature (b in equation 3.1), in contradiction with experiment[2]. Physically, the linear temperature dependence arises from the thermal depletion of the condensate near the nodes of the order parameter, and the doping dependence arises from counting the total number of electrons available to the superfluid density. The central theoretical problem appears to lie in constructing a model that would make only a small fraction $\sim x$ of all the electrons participate in the superconducting condensate while at the same time preserve the simple BCS character of the nodal quasiparticles.

Recently, very difficult experimental challenges have been overcome, and data at the lowest superconducting doping levels are finally available[2, 3]. Careful studies of the c-axis penetration depth at a number of doping values were performed, all on the same experimental sample. This incredible sample preparation technique involves changing the transition temperature of a single crystal of YBCO by room temperature annealing[18], and beautifully overcomes any extrinsic chemical effects that could arise when studying independently prepared samples.

[2]This trend has been contradicted in recent experiments [17]. How this affects this research is discussed at the end of this chapter.

In this chapter we[3] calculate the superfluid density in two scenarios. To introduce our notation and techniques, we first calculate the response of d-wave superconductors to electomagnetic fields applied perpendicular to the copper oxygen planes, using the Hamiltonian 2.28. The resulting "in-plane" superfluid density gives good agreement with experimental data, and historically gave some of the first evidence of the unconventional nature of cuprate superconductivity.

We then calculate the response of an electromagnetic field applied along the copper-oxygen planes, by postulating a Hamiltonian governing the interplanar tunneling of electrons. This results in a theoretical prediction to be compared with the aforementioned c-axis penetration depth measurements. The agreement between the theory and experiment is striking, and we conclude this chapter with a discussion of what can be gleaned from these fits, and what clues this research provides towards the final theory of high temperature superconductivity.

3.1 In-Plane Superfluid Density

The starting point for the calculation is the phenomenological cuprate Hamiltonian 2.28 written in second quantized form

$$H_0 = \sum_k \psi_k^\dagger \left[\epsilon(k)\sigma_3 + \Delta(k)\sigma_1\right]\psi_k. \tag{3.2}$$

In order to calculate the current we apply the minimal coupling prescription to the bare Hamiltonian [4]

$$H_A = H_0\left(\epsilon(k) \rightarrow \epsilon\left(k - eA(r,t)\right)\right), \tag{3.3}$$

which is then expanded to second order $H_A = H_0 + H_1 + H_2$, after taking the Fourier transform of the vector potential $A(q,t) = \int \mathrm{d}^2 r A(r,t)$. The terms in the expansion are given by[5]

$$H_1 = -e\sum_k A_i(q,t)\frac{\partial\epsilon(k)}{\partial k_i}\psi_{k+q}^\dagger \mathbb{1}\psi_k, \tag{3.4}$$

[3]The active voice will be used in this thesis whenever novel material is being discussed.

[4]For complete details in extending the minimal coupling prescription to second quantized Hamiltonians, please see appendix A.

[5]The Einstein summation convention is used, where summation is implied over any repeated indices. For example $a_i\partial_i b_j$ represents $\sum_i a_i\partial_i b_j$.

and

$$H_2 = \frac{e^2}{2}\sum_{kq}\left(A_i(p,t)\frac{\partial}{\partial k_i}\right)\left(A_j(q,t)\frac{\partial}{\partial k_j}\right)\epsilon(k)\psi^\dagger_{k+p+q}\sigma_3\psi_k. \quad (3.5)$$

The current can now be found by taking a functional derivative with respect the the vector potential

$$j_\alpha(x,t) \equiv \frac{\delta H_A}{\delta A_\alpha(x,t)}, \quad (3.6)$$

which naturally separates into two components; a paramagnetic current, coming from the Hamiltonian 3.4, and a diamagnetic current, coming from the Hamiltonian 3.5.

The current must be averaged quantum mechanically and thermodynamically, both of which can be performed simultaneously in the Matsubara formalism, as described in the last chapter.

The diamagnetic current, already proportional to the vector potential, requires only the bare Hamiltonian 3.2 in performing the quantum-thermal average

$$\langle j^D_\alpha(k',\tau)\rangle = e^2\sum_{kq}A_i(q,\tau)\frac{\partial}{\partial k_i}\frac{\partial}{\partial k_\alpha}\epsilon(k)\langle\psi^\dagger_{k+q+k'}(\tau)\sigma_3\psi_k(\tau)\rangle, \quad (3.7)$$

resulting in the expression

$$\langle j^D_\alpha(k',i\Omega)\rangle = e^2A_i(k',i\Omega)\sum_k\frac{\partial}{\partial k_i}\frac{\partial}{\partial k_\alpha}\epsilon(k)\frac{1}{\beta}\sum_n \mathrm{Tr}\mathcal{G}(k,\omega_n)\sigma_3. \quad (3.8)$$

The paramagnetic current, on the other hand,

$$\langle j^P_\alpha(k',\tau)\rangle = -e\sum_k\frac{\partial\epsilon(k)}{\partial k_\alpha}\langle\psi^\dagger_{k+k'}(\tau)\mathbb{1}\psi_k(\tau)\rangle \quad (3.9)$$

requires the Hamiltonian 3.4 in order for the average to be proportional to the vector potential:

$$\langle j^P_\alpha(k',\tau)\rangle = -e\sum_k\frac{\partial\epsilon(k)}{\partial k_\alpha}\langle e^{i\int_0^\beta H_1(\tau')\mathrm{d}\tau'}\psi^\dagger_{k+k'}(\tau)\mathbb{1}\psi_k(\tau)\rangle, \quad (3.10)$$

$$= e^2A_j(k',i\Omega)\sum_k\frac{\partial\epsilon}{\partial k_\alpha}\frac{\partial\epsilon}{\partial k_j} \times\frac{1}{\beta}\sum_n\mathrm{Tr}\mathcal{G}(k,i\omega_n)\mathcal{G}(k+k',i\omega_n-i\Omega). \quad (3.11)$$

Combining the two expressions results in the total current

$$\langle j_i(k', i\Omega)\rangle = [D_{ij} + \Pi_{ij}(k', i\Omega)]\, A_j(k', i\Omega), \tag{3.12}$$

where the two functions

$$D_{ij} \equiv e^2 \sum_k \frac{\partial}{\partial k_i}\frac{\partial}{\partial k_j}\epsilon(k)\frac{1}{\beta}\sum_n \mathrm{Tr}\mathcal{G}(k, i\omega_n)\sigma_3 \tag{3.13}$$

and

$$\Pi_{ij}(k', i\Omega) \equiv e^2 \sum_k \frac{\partial\epsilon(k)}{\partial k_i}\frac{\partial\epsilon(k)}{\partial k_j}\frac{1}{\beta}\sum_n \mathrm{Tr}\mathcal{G}(k, i\omega_n)\mathcal{G}(k + k', i\omega_n - i\Omega) \tag{3.14}$$

are related to the superfluid density

$$\rho_s^{ij}(T) \propto -D_{ij} - \lim_{\Omega\to 0} \Re\left\{\Pi_{ij}(k = 0, \Omega)\right\}. \tag{3.15}$$

It is important to note that, analogous to the conductivity, the superfluid density is a tensor. We only need the diagonal terms, however, when making a comparison with experiment.

Performing the Matsubara sums results in an expression for the superfluid density

$$\begin{aligned}\rho_s(T) \propto & \sum_k \frac{\partial^2\epsilon(k)}{\partial k_x^2}\left(1 - \frac{\epsilon(k)}{E(k)}\tanh\frac{1}{2}\beta E(k)\right) \\ & -\beta\sum_k \left(\frac{\partial\epsilon(k)}{\partial k_x}\right)^2 \mathrm{sech}^2\frac{1}{2}\beta E(k)\end{aligned} \tag{3.16}$$

An equivalent expression

$$\begin{aligned}\rho_s(T) \propto & \sum_k \left[\left(\frac{\partial\epsilon(k)}{\partial k_x}\right)^2 \frac{\Delta^2(k)}{E^2(k)} - \frac{\partial\epsilon(k)}{\partial k_x}\frac{\partial\Delta(k)}{\partial k_x}\frac{\Delta(k)\epsilon(k)}{E^2(k)}\right] \\ & \times\left[\frac{1}{E(k)} - \frac{\partial}{\partial k_x}\right]\tanh\frac{1}{2}\beta E(k).\end{aligned} \tag{3.17}$$

can be derived by an integration of 3.16 by parts. The expression 3.17 is more natural, in the sense that it explicitly vanishes in the $\Delta \to 0$ limit.

By the very nature of superconductivity, the gap always forms exactly at the Fermi surface. The unconventional d-wave symmetry of the cuprate gap 2.30 necessitates the appearance of "nodes" – points on the Fermi surface where the energy gap vanishes. Quasiparticle excitations of arbitrarily low energy exist near these nodes, and it is these quasiparticles that dominate the low energy properties of cuprate superconductors. Therefore, when calculating the low energy behaviour of the cuprates, the quasiparticle energy (measured relative to the Fermi energy) can be written

$$E^2\left(k = k_F + p\right) = \frac{1}{2}\sum_{ij} p_i p_j \frac{\partial}{\partial k_i}\frac{\partial}{\partial k_j} E^2(k = k_F) \tag{3.18}$$

$$= q_1^2 v_F^2 + q_2^2 v_\Delta^2, \tag{3.19}$$

where we have defined the nodal momentum variables

$$q_{1,2} = \frac{1}{\sqrt{2}}(p_x \pm p_y), \tag{3.20}$$

the Fermi velocity

$$v_F = \left.\frac{\partial \epsilon}{\partial k}\right|_{k_F}, \tag{3.21}$$

and the gap velocity

$$v_\Delta = \left.\frac{\partial \Delta}{\partial k}\right|_{k_F}. \tag{3.22}$$

The final form of the energy contour is an anisotropic Dirac cone.

Determining the temperature dependence of 3.17 in the nodal approximation yields the following integral

$$\rho_s^{ab}(0) - \rho_s^{ab}(T) \propto \frac{v_F}{v_\Delta}\int_0^\infty \frac{\mathrm{d}k}{4\pi}\frac{\beta k}{2}\mathrm{sech}^2\frac{\beta k}{2}, \tag{3.23}$$

which converges over the entire Brillouin zone, and therefore we can take the upper limit to infinity without introducing any significant error. The integral is now elementary, resulting in the temperature dependence of the superfluid density seen in experiments on extremely clean cuprate superconductors [12]

$$\rho_s^{ab}(0) - \rho_s^{ab}(T) \propto \frac{v_F}{v_\Delta} 4T \ln 2, \tag{3.24}$$

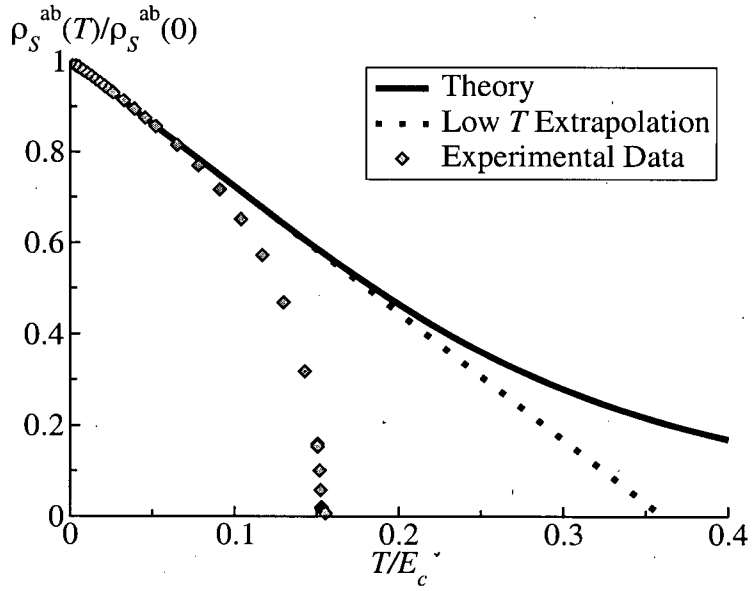

Figure 3.1: Comparison between the temperature dependence of the experimental superfluid density and theoretical calculation assuming a d-wave order parameter. The data set represents the penetration depth in the ab-plane of an optimally doped sample of YBCO with a $T_C = 60$K, taken from [1].

the low temperature agreement can be vividly seen in figure 3.1.

The zero temperature value, however, does not agree with experimental phenomenology. Analysis of the zero temperature limit of equation 3.17 reveals that $\rho_s^{ab}(0)$ should scale as the total number of electrons, or $(1-x)$ in terms of the doping parameter. Experimentally the opposite behaviour is seen. Experiments carried out using muon spin rotation over a large range of doping reveal that $\rho_s^{ab}(0)$ is directly proportional to the doping parameter x [19].

However, we do not expect the pure BCS d-wave Hamiltonian to apply across the entire phase diagram. As doping is decreased to the edge of the superconducting phase, the highly correlated Mott insulating state will certainly cast its shadow on the superconducting properties. To mimic these effects, a new term is added to the BCS Hamiltonian

$$H = H_{\mathrm{BCS}} + H_{\mathrm{Int}}, \tag{3.25}$$

where H_{Int} is left completely uncertain. However, all is not lost. The overall effect of H_{Int} will be deduced from experimental phenomenology, which will put constraints on the underlying theory of high T_C cuprates.

A parsimonious way to continue is to simplify the effect of the interactions into a "charge renormalization", inspired by the work of Ioffe and Millis [20]. Contrary to a Fermi liquid, where the electric charge is a conserved quantity, the quasiparticles that diagonalise the BCS Hamiltonian (so called 'Bogolons') do not have a definite charge and consequently are not protected against charge renormalization. The entire effect of H_{Int} will be modeled by the replacement

$$\sum_k e \rightarrow \sum_k Z_k e \tag{3.26}$$

where the momentum dependent charge renormalization factor takes the form

$$Z_k = \begin{cases} 1 & E(k) < E_c \\ 0 & E(k) > E_c. \end{cases} \tag{3.27}$$

where E_c is a doping dependent parameter that will be extracted from the data. Incorporation of the charge renormalization leads to the low-T superfluid density

$$\rho_s^{ab}(T) \approx E_c - 4T \ln 2, \tag{3.28}$$

where we can now infer the doping dependence $E_c \propto x$ from experiment [12, 19]. At this point, the seemingly ad hoc introduction of the momentum dependent charge renormalization is far from satisfying. In the next section, we will see that the same replacement also accurately describes the physics of the electronic current along the c-axis arising from interlayer tunneling.

3.2 C-Axis Superfluid Density

In order to calculate the c-axis superfluid density, the interplanar coupling Hamiltonian

$$H_c = \sum_m \int \mathrm{d}r \left(t_r c^\dagger_{rm\sigma} c_{rm+1\sigma} + t^*_r c^\dagger_{rm+1\sigma} c_{rm\sigma} \right), \tag{3.29}$$

is introduced, where the electron creation operators have been augmented with a planar index m. Without specifying the hopping matrix elements t_r, this Hamiltonian is quite general. However, by using empirical observations, a number of properties can be discerned. First, by the absence of a linear term in the c-axis superfluid density, it is known that there is no coherent tunneling between the planes[21]. This translates into the condition

$$\bar{t}_r = 0, \tag{3.30}$$

where the bar now corresponds to averaging over all realizations of disorder. Were this not the case, the Hamiltonian 3.29 would correspond to an anisotropic three dimensional superconductor.

Secondly, the empirical data obtained in 2002 on extremely pure, extremely underdoped samples were best fit[2, 3] by

$$\rho^c_s(T) \approx Ax^\alpha - BT^\alpha, \tag{3.31}$$

where mysteriously, $\alpha \approx 2.4$. While there are many theoretical proposals that predict integer power laws in the superfluid density[22], a non-integer power law is difficult to justify. The main thesis proposed here is that this is not a pure power law behaviour, but a crossover of two different regimes. The details of the crossover are dictated by the anisotropy of the energy dispersion inherent in high temperature superconductors.

The calculation begins with the usual definition of Nambu spinors, again augmented by a planar index

$$\psi_{rm} = \begin{pmatrix} c_{rm\uparrow} \\ c^\dagger_{rm\downarrow} \end{pmatrix}, \tag{3.32}$$

where now the tunneling Hamiltonian 3.29 becomes[6]

$$H_c = \sum_m \int \mathrm{d}r \left[\psi^\dagger_{rm} \left(t_r \sigma_\uparrow + t^*_r \sigma_\downarrow \right) \psi_{rm+1} + \psi^\dagger_{rm+1} \left(t^*_r \sigma_\uparrow + t_r \sigma_\downarrow \right) \psi_{rm} \right]. \tag{3.33}$$

In a tunneling Hamiltonian, the usual minimal substitution is implemented by the Peierls substitution [23], which augments the hopping matrix element by an imaginary phase equal to the line integral of the vector potential along the path of the electron

$$t_r \rightarrow t_r e^{ie \int_x^y \mathrm{d}z A(z,m,t)} \tag{3.34}$$

$$= t_r e^{iaeA_z(r,m,t)}. \tag{3.35}$$

The Hamiltonian, expanded to second order in the vector potential, becomes

$$H_c = \sum_m \int \mathrm{d}r t_r \left\{ \psi^\dagger_{rm} \sigma_3 \psi_{rm+1} + ieA_z(r,m,t) \psi^\dagger_{rm} \mathbb{1} \psi_{rm+1} - \frac{e^2}{2} a^2 A_z^2(r,m,t) \psi^\dagger_{rm} \sigma_3 \psi_{rm+1} + \mathrm{h.c.} \right\}. \tag{3.36}$$

The c-axis current

$$j_z(r,m,t) \equiv \frac{\partial H_c}{\partial A_z(r,m,t)}, \tag{3.37}$$

$$= ieat_r \left(\psi^\dagger_{rm} \mathbb{1} \psi_{rm+1} - \psi^\dagger_{rm+1} \mathbb{1} \psi_{rm} \right) - e^2 a^2 A_z(r,m,t) t_r \left(\psi^\dagger_{rm} \sigma_3 \psi_{rm+1} + \psi^\dagger_{rm+1} \sigma_3 \psi_{rm} \right) \tag{3.38}$$

can be broken into diamagnetic and paramagnetic parts,

$$j^P_z(r,m,t) = ieat_r \left(\psi^\dagger_{rm} \mathbb{1} \psi_{rm+1} - \psi^\dagger_{rm+1} \mathbb{1} \psi_{rm} \right), \tag{3.39}$$

$$j^D_z(r,m,t) = -e^2 a^2 A_z(r,m,t) t_r \left(\psi^\dagger_{rm} \sigma_3 \psi_{rm+1} + \psi^\dagger_{rm+1} \sigma_3 \psi_{rm} \right), \tag{3.40}$$

[6]The combinations $\sigma_\uparrow = \frac{1}{2}(\mathbb{1} + \sigma_3)$ and $\sigma_\downarrow = \frac{1}{2}(\mathbb{1} - \sigma_3)$ are employed.

in analogy with the in-plane calculation.

The evolution of the diamagnetic current is given by the bare tunneling Hamiltonian 3.33 with result

$$\begin{aligned}\langle j_z^D(Q,i\Omega)\rangle &= 2e^2a^2\sum_{Kpq}A(K)Z_kZ_pt_{Q-K+p-q}t^*_{p-q}\\ &\times\frac{1}{\beta}\sum_n \mathrm{Tr}\mathcal{G}(q,i\omega_n)\sigma_3\mathcal{G}(p,i\omega_n-i\Omega)\sigma_3, \qquad (3.41)\end{aligned}$$

and the evolution of the paramagnetic current is given by the first order Hamiltonian 3.36 with result

$$\begin{aligned}\langle j^P(Q,i\Omega)\rangle &= -2e^2a^2\sum_{Kpq}A(K)Z_kZ_pt_{Q+p-q}t^*_{p-q+K}\\ &\times\frac{1}{\beta}\sum_n \mathrm{Tr}\mathcal{G}(p,i\omega_n)\mathcal{G}(k,i\omega_n-i\Omega), \qquad (3.42)\end{aligned}$$

where the charge renormalization factor 3.27 has been implemented. Equations 3.41 and 3.42 both result from a perturbative expansion in the vector potential, which is equivalent to expanding in the number of tunneling events. The propagators $\mathcal{G}(p,\omega_n)$ are therefore the Green's function of the planar Hamiltonian 3.2.

The specific form of the interplane hopping matrix element t_r depends sensitively on the local chemical environment. Statistically, however, the variation of this quantity from location to location is not important, due to the self-averaging nature of experiments – an average over all realizations of disorder naturally occurs over the macroscopic size of the experimental sample. Therefore, only the disorder-averaged quantity will be of interest when making experimental comparisons, which is chosen to be

$$\overline{t_pt^*_{p+k}} = \frac{4\pi t_\perp^2}{\Lambda^2}\delta(k)e^{-p^2/\Lambda^2} \qquad (3.43)$$

where Λ is an inverse correlation length, specifying a length inside which coherence is maintained between successive interplanar hops[7].

[7]The salient feature of this choice is that it reduces to a delta function in the limit $\Lambda \gg p$. Any other form that obeys this property will not qualitatively change our conclusions.

The superfluid density can now be read directly from the disorder-averaged current

$$\langle j_z(Q,i\Omega)\rangle = 2e^2a^2A(Q)\sum_{pk} Z_kZ_p\overline{t_{p-k}t^*_{p-k}}\left[\frac{1}{\beta}\sum_n \mathrm{Tr}\mathcal{G}(k,i\omega_n)\mathcal{G}(p,i\omega_n-i\Omega)\right.$$
$$\left.-\frac{1}{\beta}\sum_n \mathrm{Tr}\mathcal{G}(p,i\omega_n)\sigma_3\mathcal{G}(k,i\omega_n-i\Omega)\sigma_3\right], \tag{3.44}$$

with result

$$\rho_s^c(T) = 4a^2\sum_{pk} Z_kZ_p\overline{t_{p-k}t^*_{p-k}}\frac{\Delta(p)\Delta(k)}{E(p)E(k)}$$
$$\times\left\{\frac{E(k)\tanh\frac{1}{2}\beta E(p)-E(p)\tanh\frac{1}{2}\beta E(k)}{E^2(p)-E^2(k)}\right\}. \tag{3.45}$$

The superfluid density 3.45 must be integrated numerically to compare against the experimental data [2, 3]. The dependence of the superfluid density on temperature and doping must be calculated independently. The temperature dependence can be found by subtracting off the zero temperature value, which amounts to replacing the hyperbolic tangent functions with $(1-\tanh)$. To proceed further, we linearize the spectrum, switch to relative $q=(k-p)/2$ and centre-of-mass $Q=(p+k)/2$ coordinates, and scale the momentum coordinates $Q_1\to v_FQ_1$, $Q_2\to v_\Delta Q_2$ (similarly for q). In dimensionless form, the superfluid density becomes

$$\rho_s^c(0)-\rho_s^c(T) = 16\pi^2a^2\frac{\Lambda t_\perp^2}{\sqrt{v_Fv_\Delta}}I_1(\tau,\eta), \tag{3.46}$$
$$I_1(\tau,\eta) = 4\tau^3\int \mathrm{d}^2q e^{-4\tau^2(q_1^2/\eta-q_2^2\eta)}\Omega(q), \tag{3.47}$$

where

$$\Omega(q) = \frac{1}{4}\int \mathrm{d}^2Q\frac{q_2^2-Q_2^2}{|Q+q||Q-q|}\frac{1}{q\cdot Q}\left[|Q-q|\left(1-\tanh\frac{|Q+q|}{2}\right)\right.$$
$$\left.-|Q+q|\left(1-\tanh\frac{|Q-q|}{2}\right)\right] \tag{3.48}$$

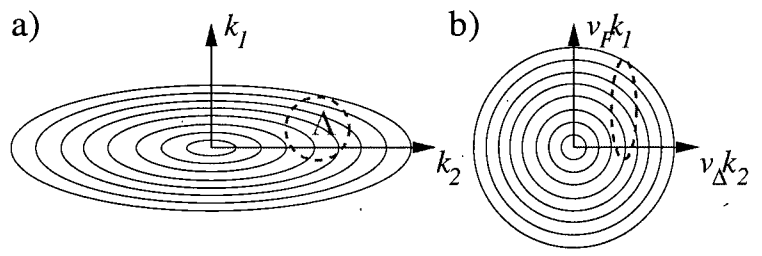

Figure 3.2: Schematic of the constant energy contours in momentum space in the vicinity of a node. On the left, contours at energy $E(k)$ satisfy $E^2(k) = v_F^2 k_1^2 + v_\Delta^2 k_2^2$. The tunneling matrix element conserves momentum within a range Λ represented by the dashed circle. By rescaling the plot so that the axes are $v_F k_1$ and $v_\Delta k_2$, the constant energy contours are circles, but the circle representing the degree of momentum conservation has become distorted, indicating that the k_1 component of the quasiparticle momentum is effectively conserved to a lesser degree than k_2.

and the integrals have been written in terms of a dimensionless temperature variable $\tau = T/\sqrt{v_F v_\Delta}\Lambda$ and anisotropy parameter $\eta = v_F/v_\Delta$. The domain of integration in 3.47 can be safely taken to be infinite, as the temperature plays the role of a cutoff in this calculation.

The rescaling of the momentum coordinates plays a crucial role in understanding the mysterious non-integer power law behaviour of the data. Recalling that the chemical disorder mediates electron hops between copper-oxygen planes, the in-plane momentum is conserved in a momentum region of order Λ, as seen in equation 3.43. Rescaling the momentum coordinates produces an isotropic energy spectrum, but renders the hopping matrix element anisotropic, in such a way that the q_1 component of the quasiparticle momentum is conserved to a lesser degree than q_2, as seen in figure 3.2. The temperature must be compared to the two new energy scales in the problem $v_F\Lambda$ and $v_\Delta\Lambda$.

At high temperature $v_\Delta\Lambda \ll v_F\Lambda \ll T$, the hopping matrix element 3.43 becomes coherent, the momentum is completely conserved while hopping between planes. This leads to a linear behaviour in the superfluid density (as this calculation will follow exactly as the in-plane calculation). In the intermediate region $v_\Delta\Lambda \ll T \ll v_F\Lambda$, the hopping matrix element can be viewed as conserving only the q_2 component of the momentum, while q_1 is completely

unrestricted. Power counting in 3.47 results in a quadratic temperature dependence. Finally, in the low-temperature limit $T \ll v_\Delta \Lambda \ll v_F \Lambda$, the momentum is completely non-conserved, naively giving a flat temperature dependence. However, a careful asymptotic analysis of the integral $I_1(\tau, \eta)$ reveals a cubic temperature dependence [24]. Summarizing

$$\rho_s^c(0) - \rho_s^c(T) \approx \begin{cases} T^3 & T \ll v_\Delta \Lambda \ll v_F \Lambda \\ T^2 & v_\Delta \Lambda \ll T \ll v_F \Lambda \\ T & v_\Delta \Lambda \ll v_F \Lambda \ll T \end{cases} . \tag{3.49}$$

The doping dependence can be calculated in a similar fashion, with result

$$\rho_s^c(0) = 16\pi^2 e^2 a^2 \frac{\Lambda t_\perp^2}{\sqrt{v_F v_\Delta}} I_2(\epsilon_C, \eta), \tag{3.50}$$

$$I_2(\epsilon_C, \eta) = \epsilon_C^3 \int_1 \mathrm{d}^2k \mathrm{d}^2p \frac{k_2 p_2}{kp} \frac{1}{k+p} e^{-\epsilon_C^3 [(k_1-p_1)^2/\eta - (k_2-p_2)^2 \eta]}, \tag{3.51}$$

where the subscript on the integration measure indicates that the integration range is the unit disk, corresponding to the choice of Z_k, and $\epsilon_C = E_c / \sqrt{v_F v_\Delta} \Lambda$. In practice, for numerical convenience we shall replace this hard cutoff with a Gaussian soft cutoff when performing numerical integrals[8].

In the zero-temperature superfluid density, the cutoff energy plays the analogous role as temperature above. The only change is that the asymptotic expansion of $I_2(\epsilon_C, \eta)$ produces a quintic low-ϵ_C behaviour. Therefore

$$\rho_s^c(0) \approx \begin{cases} E_c^5 & E_c \ll v_\Delta \Lambda \ll v_F \Lambda \\ E_c^2 & v_\Delta \Lambda \ll E_c \ll v_F \Lambda \\ E_c & v_\Delta \Lambda \ll v_F \Lambda \ll E_c \end{cases} , \tag{3.52}$$

and the apparent non-integer power law seen experimentally is a result of a crossover between different integer power laws, based solely on the natural anisotropy inherent in cuprate superconductors.

3.3 Comparison with Experiment

In order to compare the results to experimental data, we break the data into two sets: the temperature dependent superfluid density

$$\delta \rho_s^c(T) = \rho_s^c(0) - \rho_s^c(T) \tag{3.53}$$

[8] This corresponds to $Z_k = \exp\{-E_k^2/E_c^2\}$ which will not qualitatively alter the previously calculated ab-plane superfluid density.

and the zero temperature value $\rho_s^c(0)$. This procedure renders $\delta\rho_s^c(T)$ independent of the cutoff energy E_c, as required by the universal behaviour of the experimental data – all the data lie on one curve after performing this subtraction.

The temperature dependent c-axis superfluid density was numerically integrated as a function of dimensionless temperature for a number of values of the anisotropy parameter η. The results, summarized in figure 3.3, clearly show a linear behaviour for large τ, a plateau of quadratic behaviour for intermediate τ whose persistence increases with increasing anisotropy, and a cubic low temperature regime. Therefore, the behaviour across the entire temperature range is as expected from the naive power counting arguments previously presented.

The temperature dependent data fits reveal the two parameters $t_\perp$ and Λ that both characterize the way in which tunneling occurs in the c-direction. Since all of the data sets were acquired from one single sample, they are taken to be global fitting parameters. We take the usual values $v_F = 1.8\text{evÅ}$ and $d = 5.85\text{Å}$, although it is not known if v_F changes for strongly underdoped samples.

In figure 3.4 we show our best fits to the low-temperature values of $\delta\rho_s^c(T)$ in the experiments of [2, 3]. The diamonds represent the data curves for a particular doping value. Each doping value is characterized by a particular T_c that we take to be proportional to doping x. For clarity, we have only included the highest doping values $T_c = \{20.2, 19.5, 18.2, 17.8, 16.4, 15.1\text{K}\}$; the fits are equally good for lower doping values. The solid line is our best fit with the parameter $\hbar\Lambda^{-1} = 120\text{Å}$ and $t_\perp = 26\text{meV}$. The fits work well at low T (despite the fact that the data is not a simple power law) but begins to deviate at high temperature. We ascribe this discrepancy to fluctuation effects near T_c in a given sample as well as the fact that we have neglected the effect of Z_k on the finite temperature corrections to $\delta\rho_S^c(T)$ above. This restricts the validity of our calculations to low temperature.

Having fit the temperature dependent correction, the only remaining parameters are the values of E_c corresponding to a particular doping. We extract these using equation 3.51. In the last section, we noted that to account for the ab-plane phenomenology, we must take $E_c \propto x$, in figure 3.6 we plot (diamonds) the extracted best-fit values of E_c for a given experimental T_c from the data. The solid curve is a linear fit to these values, with the form $E_c = 0.49T_c/\text{K}$. This linear "Uemura" [19] relation is an important constraint on this theory and depicts the destruction of the Fermi surface as

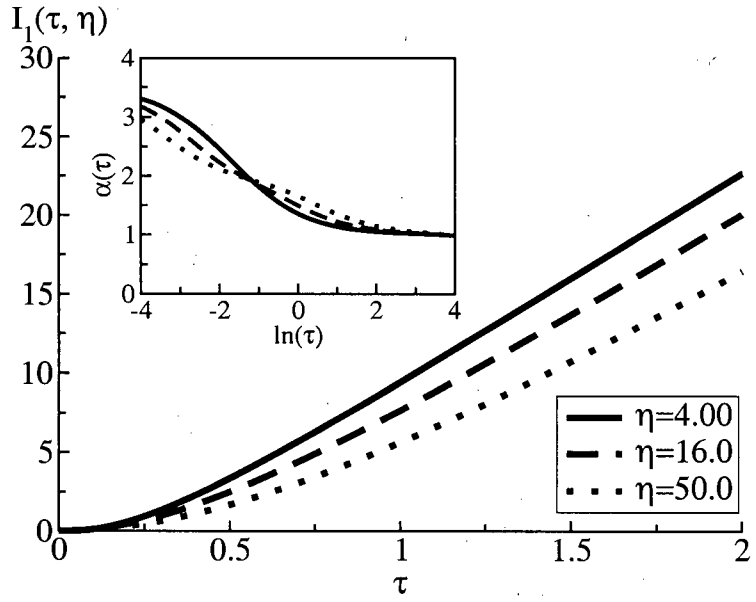

Figure 3.3: Plot of $I_1(\tau, \eta)$ for $\eta = 4, 16, 50$. To emphasize the crossover behaviour in the power law of $I_1(\tau, \eta)$, the inset plots the associated logarithmic derivative $\alpha(\tau) = d \ln I_1 / d\tau$.

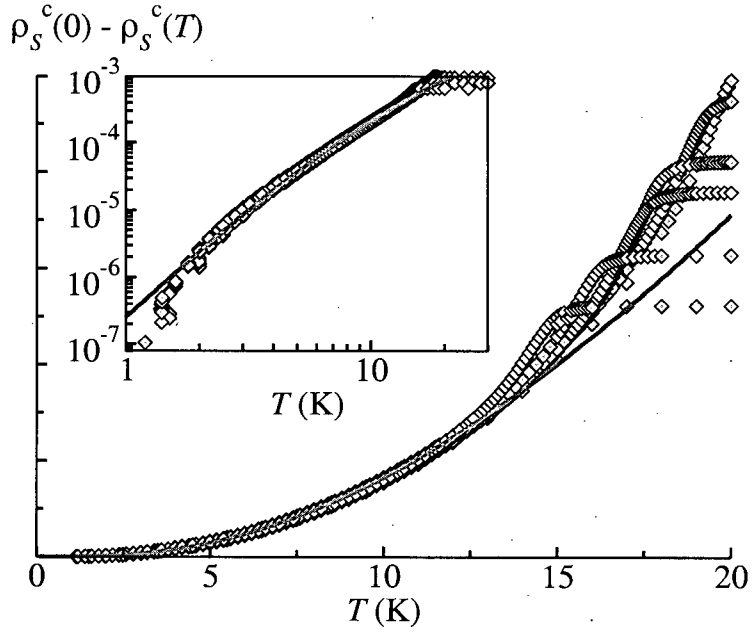

Figure 3.4: Plot of fits to experimental data of Refs. [2, 3]. The diamonds are $\delta\rho_s^c(T)$ for various dopings having experimental T_c values (top to bottom) $T_c = \{20.2, 19.5, 18.2, 17.8, 16.4, 15.1\text{K}\}$. The solid curve is our best fit using the parameters $\hbar\Lambda^{-1} = 120\text{Å}$ and $t_\perp = 26\text{meV}$. The inset is the same plot on a logarithmic scale, showing the changing power law of the experimental data and of our theoretical curve.

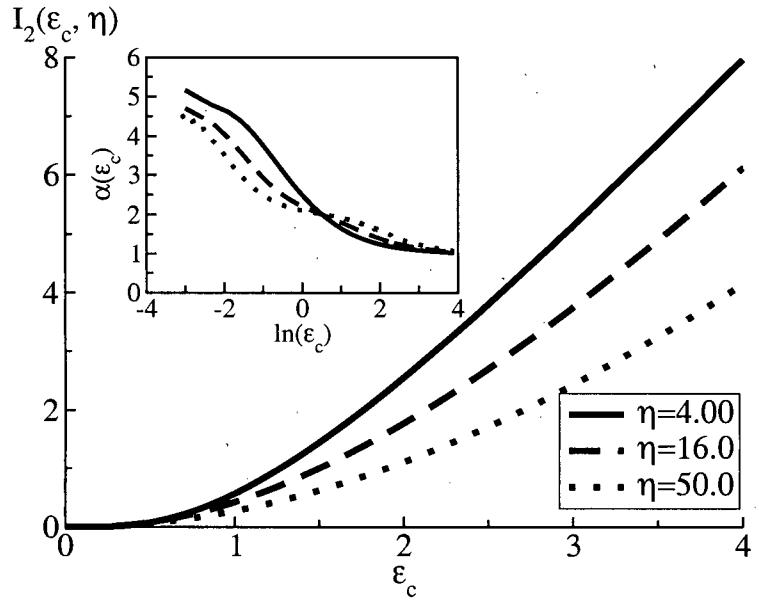

Figure 3.5: Plot of $I_2(\epsilon_C, \eta)$ for $\eta = 4, 16, 50$. To emphasize the crossover behaviour in the power law of $I_2(\epsilon_C, \eta)$, the inset plots the associated logarithmic derivative $\alpha(\epsilon_C) = d \ln I_2 / d\epsilon_C$.

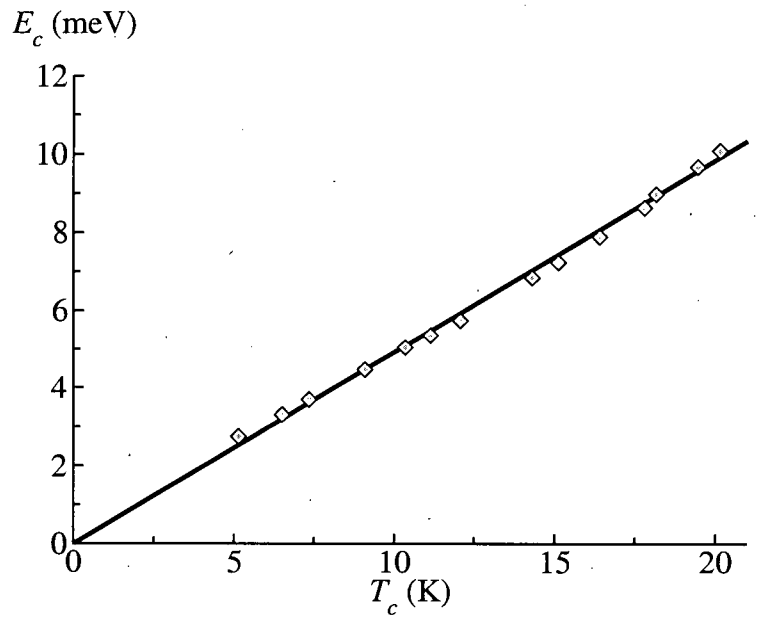

Figure 3.6: Plot of extracted values of the charge renormalization parameter $\hat{E}_c$ (diamonds) as a function of the experimental T_c, showing a linear behaviour as a function of doping level. The solid curve is a linear fit to these values, and has the form $E_c = 0.49T_c/\mathrm{K(meV)}$.

the Mott insulating phase is approached at low doping values.

Finally, to illustrate the overall agreement of our model with the data, in figure 3.7 we plot the data for several representative doping values along with our curve fits. The agreement is strikingly good at low temperatures for all doping levels. We emphasize that all data sets are fit with a single set of parameters; the only parameter that varies is the cutoff energy according to $E_c = 0.49T_c/\mathrm{K}$ with T_c being the actual measured critical value.

Recently, the zero temperature superfluid density has been carefully measured in extremely clean underdoped cuprates [17; 25]. The results are that $\rho_s^{ab}(0)$ scales sub-linearly with x for low doping. This experimental fact contradicts one of the assumptions that underlies this model. The main conclusion, however, that d-wave nodal quasiparticles qualitatively and quantitatively explain the empirically determined c-axis superfluid density of YBCO survives this modification.

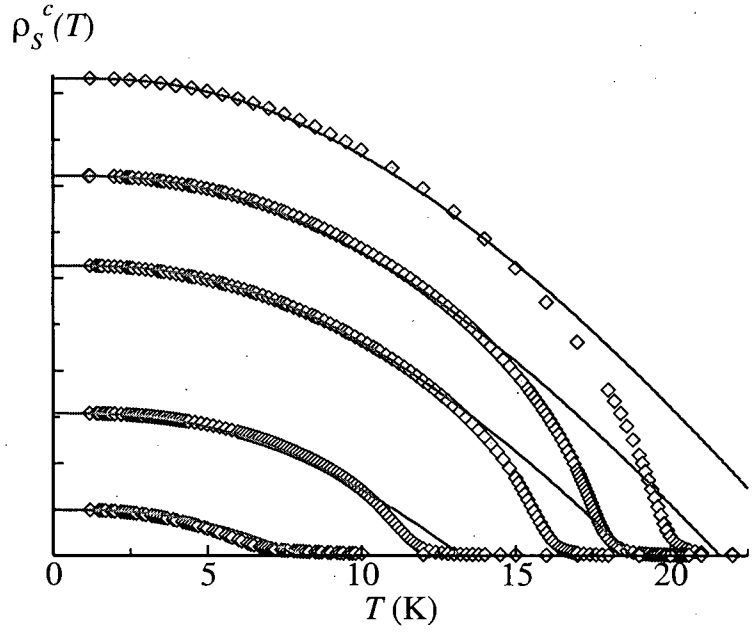

Figure 3.7: Fit to data of [2, 3] (diamonds) using parameters extracted in text. The T_c values are $T_c = \{20.2, 18.2, 16.4, 12.1, 7.4K\}$ (top to bottom) representing decreasing effective doping. The parameters used are $\hbar\Lambda^{-1} =$ 120Å, $t_\perp = 26$meV, $\eta = v_F/v_\Delta \doteq 6.8$ and $E_c = 0.49T_c$meV/K.

On the other hand, the c-axis tunneling could act as a scattering mechanism and modify the in-plane superfluid behaviour. In fact, the relatively large value of Λ implies that the leading order behaviour should be quadratic for much of the temperature range up to T_C. Although the samples investigated in [17] do not show this behaviour, our model of c-axis tunneling may still be valid in these samples, but with a much smaller value of the inverse scattering length Λ.

3.4 Conclusion

In this chapter we have examined the superfluid density in high T_C superconductors. Defined as the fraction of electrons in the sample that participate in superconductivity, the superfluid density reveals important clues concerning the nature of cuprate superconductivity. We have presented a calculation describing the electromagnetic response of cuprate superconductors to field applied perpendicular to the copper-oxygen planes. The resulting linear depletion of the superfluid density with increasing temperature gives conclusive evidence of the d-wave symmetry of the superconducting order parameter. The behaviour of the zero temperature superfluid density, however, remained mysterious. We have shown that this behaviour can be parsimoniously explained by postulating that the number of electrons that can participate in superconductivty decreases linearly with doping, and furthermore that these electrons all exist in the region of the Brillouin zone surrounding the node of the d-wave order parameter.

This mysterious conclusion is further supported by experimental data first presented in the Ph.D. thesis of Ahmed Hosseini in 2000 at the University of British Columbia. Measurements were performed on extremely underdoped samples with the novel feature that the transition temperature of a single sample could be tuned continuously. The electromagnetic response to fields applied along the direction of the copper-oxygen planes was measured at various, extremely low transition temperatures.

The data collected had two remarkable properties: the data was universal, it all collapsed onto one universal curve after subtracting the zero temperature superfluid density, and that the same power law governed both the temperature dependence and the doping dependence.

A number of theoretical proposals have predicted integer power law behaviour in the temperature dependence of the c-axis superfluid response.

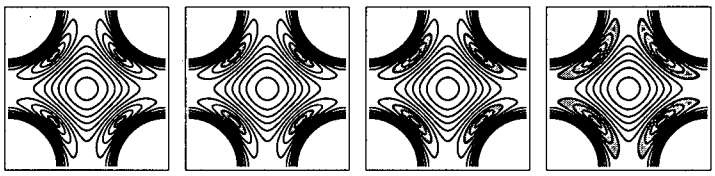

Figure 3.8: Schematic plot of the assumed form of Z_k, showing the "nodal protectorate" region (shading) of the Brillouin zone where states contribute to the formation of the condensate for a cuprate at a particular doping x. The black lines are the constant energy contours in the Brillouin zone (which do not vary with doping). Near optimal doping ($x = 20$), electrons in a large region around the node contribute to the Meissner response. As the doping is reduced this region is progressively reduced, leaving a small "patch" near the nodes where the superconductivity remains robust. We remark that the c-axis penetration depth measurements of Refs.[2, 3] were performed on extremely underdoped samples with effective dopings x that are approximately represented by the leftmost panel.

Careful consideration of the copper and oxygen atomic orbitals that mediate interplanar tunneling predict a quintic power law [22]. This behaviour cannot be ruled out by the experimental data, but, if present, it is overwhelmed by the nearly quadratic power law at low temperature.

A similar model containing disorder mediated incoherent tunneling predicts a quadratic power law [26]. However, this model assumes that the interplanar tunneling matrix element depends only on the component of the momentum parallel to the Fermi surface, implying that the momentum perpendicular to the Fermi surface is not conserved. It is not easy to imagine an interlayer scattering mechanism that would produce tunneling that is perfectly conserving for the momentum parallel to the Fermi surface while totally nonconserving in the perpendicular direction. However, any model that predicts a pure integer power law has been ruled out by the experimental data.

By introducing a momentum scale Λ, our model naturally accounts for all of these properties. The non-integer power law arises as a crossover between different integer regimes, depending on the temperature, and the cutoff energy. The momentum conservation along the direction of the Fermi surface is

naturally explained by the rescaling of the anisotropic interplanar tunneling matrix element into the nodal coordinates.

Taken together, the above results lead to the notion of a "nodal protectorate" in which coherent BCS quasiparticles persist even as the system approaches the Mott insulating state near half filling. The nodal protectorate is schematically illustrated in figure 3.8. The existence of the nodal protectorate imposes a number of stringent constraints on any microscopic theory describing the underdoped regime. In particular, any such theory must explain what protects the low-energy nodal excitations from the strong interactions that otherwise drive the electrons in the remainder of the Brillouin zone inert to applied electromagnetic fields.

Chapter 4

Macroscopic Quantum Behaviour in Cold Atomic Gases

The implications that equation 2.10

$$|\psi_B(1;2)\rangle = +|\psi_B(2;1)\rangle \tag{4.1}$$

have on the statistical behaviour of a many-body system were not fully realized until Einstein extended the revolutionary ideas of the great Indian physicist Satyendra Bose. Einstein proposed that the new statistics Bose discovered to expalain light quanta, may also be applied to particles of integer spin. This implied that a thermodynamic phase transition takes place at an extremely low temperature, where all of the particles fall into a single quantum mechanical state of matter. The resulting "Bose-Einstein Condensate" (BEC) has the remarkable property that all $N \approx 10^5$ particles can be described by a single macroscopic quantum wavefunction (or order parameter). It took seventy years for this prediction to be borne out in the laboratory: in 1995 two groups, American physicists Eric Cornell and Carl Wieman at the University of Colorado, Boulder, and a German physicist Wolfgang Ketterle at the Massachusetts Institute of Technology, realized the Bose-Einstein condensate with cold atomic gases.

4.1 Introduction to Bose-Einstein Condensation

The key principle in statistical mechanics is that the probability of a system to be in a particular microstate is given by the expression

$$p_i = \frac{1}{\mathcal{Z}} e^{-\beta E_i}, \tag{4.2}$$

where the partition function

$$\mathcal{Z} = \sum_i e^{-\beta E_i} \tag{4.3}$$

is defined as the sum of all the thermal Boltzmann factors of the corresponding microstates of the system. However, if the system contains a large number of particles whose total is fixed, the resulting partition function

$$\mathcal{Z} = \sum_{\{n_i\}} e^{-\beta \sum_i n_i E_i}, \tag{4.4}$$

where n_i is the number of particles in a given microstate, becomes extremely difficult to sum, due to the constraint on the number of particles $N = \sum_i n_i$.

This difficulty is removed by considering the grand partition function, where the total number of particles N is no longer held fixed, but allowed to fluctuate. A Lagrange multiplier is consequently added to the system, whose value can be tuned to keep the average number of particles fixed at N. Physically, this can be thought of as allowing the system to be connected with a particle reservoir, that can freely exchange particles with the system. The Lagrange multiplier μ is in principle controllable, for example by a voltage difference applied across the reservoir/system, and is known as the "chemical potential".

In the presence of the chemical potential, the partition function becomes

$$\mathcal{Z} = \prod_i \sum_{n_i} e^{-\beta n_i (E_i - \mu)} \tag{4.5}$$

and can be easily summed

$$\mathcal{Z} = \prod_i \left(\frac{1}{1 - e^{-\beta(E_i - \mu)}} \right) \tag{4.6}$$

for Bosonic particles. Various thermodynamic quantities can be found by taking logarithmic derivatives of the partition function. For example the particle number is given by

$$\langle N \rangle = \frac{1}{\beta} \frac{\partial \ln \mathcal{Z}}{\partial \mu}, \tag{4.7}$$

and the energy

$$\langle E\rangle - \mu\langle N\rangle = -\frac{\partial \ln \mathcal{Z}}{\partial \beta}. \tag{4.8}$$

The salient features of Bose-Einstein condensation can be seen in the ideal gas, with the free energy dispersion $E(k) = \frac{k^2}{2m}$, in arbitrary dimension d. The particle density

$$\begin{aligned} \rho &\equiv \frac{\langle N\rangle}{V}, \\ &= -\frac{1}{\beta}\sum_i \frac{\partial}{\partial \mu} \ln\left(1 - e^{-\beta(E_i-\mu)}\right), \\ &= \int \mathrm{d}E \frac{e^{-\beta(E-\mu)}}{1-e^{-\beta(E-\mu)}} D(E), \end{aligned} \tag{4.9}$$

where the density of states

$$D(E) = \left(\frac{m}{2\pi}\right)^{\frac{d}{2}} \frac{1}{\Gamma\left(\frac{d}{2}\right)} E^{\left(\frac{1}{2}d-1\right)} \tag{4.10}$$

has been introduced, can be written in the closed form

$$\rho = \left(\frac{m}{2\pi}\right)^{\frac{d}{2}} T^{\frac{d}{2}} \zeta_{\frac{d}{2}}(z), \tag{4.11}$$

by defining the fugacity $z = e^{\beta\mu}$ and introducing the generalized Riemann zeta function $\zeta_\alpha(z) = \sum_n \frac{z^n}{n^\alpha}$.

A similar calculation produces the average energy (measured relative to the chemical potential)

$$\begin{aligned} \epsilon &\equiv \frac{\langle E\rangle - \mu\langle N\rangle}{V} \\ &= \left(\frac{m}{2\pi}\right)^{\frac{d}{2}} \frac{d}{2} T^{\frac{d}{2}+1} \zeta_{\frac{d}{2}+1}(z), \end{aligned} \tag{4.12}$$

which can be written in terms of the density

$$\epsilon = \frac{d}{2}\rho T \frac{\zeta_{\frac{d}{2}+1}(z)}{\zeta_{\frac{d}{2}}(z)}. \tag{4.13}$$

In the high temperature limit in three dimensions, this expression reduces to the well known classical expression

$$\epsilon = \frac{3}{2}\rho T. \tag{4.14}$$

In the opposite limit, however, things start to become interesting. The series that defines the Riemann zeta function ceases to converge as $z \to 1$. At a low enough temperature (or equivalently a high enough particle density), the discrete nature of the ground state energy level becomes crucial, and replacing the summation over discrete states by an integral is no longer valid.

The number of particles in the ground state is found to be (measuring energies relative to the ground state)

$$\langle N_0 \rangle = \frac{1}{1 - e^{-\beta\mu}}, \tag{4.15}$$

which can be inverted to find the chemical potential in the limit of small temperature or large ground state filling

$$\mu \approx -\frac{T}{\langle N_0 \rangle} \ll 1. \tag{4.16}$$

The integration is still valid for states above the ground state, and the chemical potential can be neglected, giving an "excited" occupation

$$\begin{aligned} \langle N \rangle - \langle N_0 \rangle &= V \left(\frac{m}{2\pi}\right)^{\frac{d}{2}} T^{\frac{d}{2}} \zeta_{\frac{d}{2}}(1) \\ &= \langle N \rangle \left(\frac{T}{T_c}\right)^{\frac{d}{2}}, \end{aligned} \tag{4.17}$$

or more suggestively,

$$\frac{\langle N_0 \rangle}{\langle N \rangle} = 1 - \left(\frac{T}{T_c}\right)^{\frac{d}{2}}, \tag{4.18}$$

which defines the transition temperature[1]

$$T_c = \frac{2\pi}{m}\left[\frac{(2\pi)^3 \rho}{\zeta_{\frac{d}{2}}(1)}\right]^{\frac{2}{d}}. \tag{4.19}$$

[1]Convergence of the integral that leads to equation 4.17 puts limits on the dimensionality of systems that can display this phase transition. Bose condensation cannot occur in one dimension, and in two dimensions only when the trapping potential is sufficiently confining, i.e. grows with a power greater than two.

The ground state occupation can be used as a thermodynamic order parameter whose macroscopic occupation signals a phase transition into the Bose condensed state.

It is very tempting to identify the superfluid transition in Helium 4 with Bose-Einstein condensation, since the transition temperature found by inserting the relevant parameters into 4.19 is extremely close to the experimental lambda-point transition. However, it is quite clear that the Helium 4 system is far from a non-interacting Bose gas. Particle interactions, while relatively weak, cannot be neglected. In fact, superfluidity will not even occur in a non-interacting Bose gas.

Interest in the non-interacting Bose gas was rekindled when atomic physicists developed the technique of using magnetic fields to selectively confine hyperfine states of alkali gases. Combined with the discovery of laser cooling, cold atomic gases seemed like the perfect system to realize Bose-Einstein condensation.

The magnetic traps can be approximated by a harmonic confining potential. In this case, the number of excited particles in the grand canonical ensemble becomes

$$\langle N\rangle - \langle N_0\rangle = \sum_{n_x n_y n_z} \frac{1}{e^{\beta(\omega_x n_x+\omega_y n_y+\omega_z n_z)-\mu)}-1}. \tag{4.20}$$

When the particle number is great enough, the summation can be safely approximated as an integral. This amounts to a semi-classical treatment of the excited states of the harmonic oscillator. The resulting expression

$$\langle N\rangle - \langle N_0\rangle = \left(\frac{T}{\omega_0}\right)^3 \int \mathrm{d}x_1\mathrm{d}x_2\mathrm{d}x_3 \frac{1}{e^{x_1+x_2+x_3}-1}, \tag{4.21}$$

where $\omega_0 = (\omega_x\omega_y\omega_z)^{1/3}$, has solution

$$\frac{\langle N_0\rangle}{\langle N\rangle} = 1 - \left(\frac{T}{T_c}\right)^3 \tag{4.22}$$

with transition temperature

$$T_c = \omega_0 \left(\frac{N}{\zeta_3(1)}\right)^{\frac{1}{3}}. \tag{4.23}$$

To find further details of the preceeding calculation, it is performed in [27].

To achieve Bose-Einstein condensation of cold atoms, the atoms must be kept in the metastable gaseous state as the system is cooled. This necessitates a low density, since three body collisions will seed a solid state[2]. However, lowering the particle density drives down the transition temperature according to equation 4.23. Therefore the atoms must be lowered to, and maintained at, nanoKelvin temperatures. After decades of experimentation, this feat was finally achieved in 1995, when two experimental groups independently realized the Bose-Einstein condensate in cold atomic gases. The Nobel prize in 2001 was awarded for this feat to Eric Cornell, Carl Wieman and Wolfgang Ketterle.

Although the above predictions give the correct qualitative description of Bose condensation, a more sophisticated, interacting theory must be investigated in order to compare quantitatively with experiments, The starting point is the general many-body Hamiltonian

$$\begin{aligned} H &= \int \mathrm{d}r\psi^\dagger(r)\left(\frac{p^2}{2m}+V_{\mathrm{ext}}(r)\right)\psi(r) \\ &\quad +\frac{1}{2}\int \mathrm{d}r\mathrm{d}r'\psi^\dagger(r)\psi^\dagger(r')V(r-r')\psi(r')\psi(r). \end{aligned} \tag{4.24}$$

In a dilute Bosonic gas, the interaction potential can be approximated by

$$V(r-r') = \frac{4\pi a}{m}\delta(r-r'), \tag{4.25}$$

(where a is the two-body s-wave scattering length) a result that can be rigorously justified by a T-matrix calculation (see chapter 5 in [28] for a derivation). By using the Heisenberg picture[3] to derive the equations of motion for the operator $\psi(r)$, we arrive at the equation

$$i\frac{\partial}{\partial t}\hat{\psi}(r,t) = \left(-\frac{\nabla^2}{2m}+V_{\mathrm{ext}}(r)+g|\hat{\psi}(r,t)|^2\right)\hat{\psi}(r,t), \tag{4.27}$$

[2]Two body collisions cannot form a bound state since they are necessarily elastic. A third body must be present to carry away excess kinetic energy from forming a bound state.

[3]The Heisenberg equations of motion can be derived by ascribing the quantal time dependence to the operators after applying Dirac's quantization procedure to 1.11. The resulting operator equations of motion are

$$i\frac{\partial}{\partial t}\hat{\Omega} = \left[H,\hat{\Omega}\right]. \tag{4.26}$$

where we have defined the interaction parameter $g \equiv 4\pi a/m$. This operator equation of motion can be turned into a partial differential equation by a mean-field theory ansatz

$$\begin{aligned} \hat{\psi}(r,t) &\equiv \langle\hat{\psi}(r,t)\rangle + \hat{\psi}'(r,t), \\ &= \Phi(r,t) + \hat{\psi}'(r,t) \end{aligned} \tag{4.28}$$

where the operator has been split into its mean value $\Phi(r,t)$ and an operator representing fluctuations about its mean value. This separation is quite general, however it is only useful when the $\Phi(r,t)$ is large. Physically this is true when the operator $\hat{\psi}(r,t)$ represents a macroscopically filled quantum state, as is the case for the ground state in a Bose condensed system where fluctuations out of the condensate are small; $\frac{N-N_0}{N_0} \ll 1$.

If we therefore consider the equation that determines the structure and dynamics of the macroscopically occupied ground state, we arrive at the Gross-Pitaevskii (GP) equation

$$i\frac{\partial}{\partial t}\Phi(r,t) = \left(-\frac{1}{2m}\nabla^2 + V_{\text{ext}}(r) + g\Phi^2(r,t)\right)\Phi(r,t), \tag{4.29}$$

which is simply the Schrödinger equation augmented by a non-linear term due to many-body interactions, whose eigenfunctions $\Phi(r,t)$ describe various states of the many body wavefunction; the ground state, excited states including vortices and solitons, for example.

The wavefunction $\Phi(r,t)$ is given by the expectation value of a single annihilation operator, which can only be nonzero when connecting two states whose occupation number differs

$$\Phi(r,t) = \langle N|\hat{\psi}(r,t)|N-1\rangle. \tag{4.30}$$

If we ascribe the whole time dependence to that of the Fock states $|N\rangle$ then the time evolution of the condensate wavefunction is given by

$$\begin{aligned} \Phi(r,t) &= \langle N|e^{-iE_N t}\hat{\psi}(r)e^{iE_{N-1}t}|N-1\rangle \\ &= \Phi(r)e^{-i(E_N - E_{N-1})t}. \end{aligned} \tag{4.31}$$

In the limit of large particle number (which must be the case for Bose condensation to appear in the first place) the argument of the exponential approaches the chemical potential;

$$E_N - E_{N-1} \approx \frac{\partial E_N}{\partial N} = \mu. \tag{4.32}$$

Therefore the eigenvalue of the GP equation gives the chemical potential, and the time-independent GP equation reads

$$\left(-\frac{1}{2m}\nabla^2 + V_{\text{ext}}(r) + g\Phi^2(r)\right)\Phi(r) = \mu\Phi(r). \tag{4.33}$$

The Gross-Pitaevskii equations 4.29 and 4.33 give an extremely accurate description of the condensate wavefunction and its low-temperature dynamics. At temperatures close to the transition temperature, it is necessary to go beyond mean-field theory and include interaction effects between atoms in the condensate with those not in the condensate[29]. These topics are studied by keeping the second operator in equation 4.28 representing the fluctuations of particles out of the condensate. While this is an interesting and richly studied field, we will not consider this avenue further, and interested readers are directed to [29].

4.2 Cooling and Trapping of Atoms

If the time-dependent Gross-Pitaevskii equation, and the weak interactions between the condensed and non-condensed particles, encompassed the full study of cold atomic gases, the field would not have garnered the widespread attention of so many disciplines. The interest stems from a surprising result that arose from the techniques of cooling and trapping atomic gases.

The fact that the pressure of photons can be used to change the average velocity of atomic beams has been known for decades [30]. This was predicated upon the fact that an individual atom can make a transition to an excited state by an absorption of a photon. When the atom undergoes spontaneous emission the photon is emitted in a random direction. Therefore, there is a net average change in momentum after a large number of absorption-emission events. However, in order to change the temperature of an atomic gas, you need to not only change the average velocity, but narrow the velocity distribution of the ensemble. In order to accomplish this feat, the probability of photon absorption must be enhanced for atoms with a large velocity compared to those with a small velocity. This situation can be realized by shining six counter propagating lasers on the sample, each with an energy slightly detuned from the atomic energy splitting. In the frame of the moving atom, the laser energies are Doppler shifted. Since the probability of an atomic transition is proportional to the detuning parameter (at least for

a small range of velocities), the atom will favourably absorb a photon from the laser source it is traveling towards. Furthermore, the faster the atom is traveling (up to a critical velocity that will depend on the experimental details) the more likely it is to absorb a photon. The net result is the required reduction in the width of the velocity distribution.

While this "Doppler cooling" technique works very well, it has two distinct drawbacks. First, it only changes the momentum distribution of the atoms, without affecting their position. Therefore it creates what is known as "optical molasses", a region where the atoms will slow and become cool, but it provides no trapping mechanism. The second drawback is that the lowest temperature achievable using Doppler cooling is relatively large, and much higher than a typical Bose condensation temperature.

Trapping of the atomic gas was achieved by tuning the atomic energy levels in an inhomogeneous magnetic field via the Zeeman interaction. By tailoring the magnetic field lines to produce a minimum at the same location as the optical molasses, the atoms could be confined as they are being cooled. This system of using magnetically tuned energy levels in the presence of an optical molasses is known as a Magneto-Optical trap (MOT) and is currently used as the standard cooling technique used in experiments.

This heuristic description describes the cooling and trapping of a hypothetical two-level atom. In reality, atoms possess ground and excited state manifolds, containing many different energy levels that depend on internal quantum numbers. Furthermore, the strength of the electromagnetic coupling between two states will depend on the polarization of the laser via the well-known Clebsch-Gordan coefficients resulting from angular momentum conservation.

Consider two counter-propagating laser beams along the z-axis with perpendicular polarization vectors:

$$\vec{E}(z,t) = \hat{x}\cos(\omega t - kz) + \hat{y}\sin(\omega t + kz)\,. \tag{4.34}$$

At distances that are multiples of a quarter wavelength $kz = n\pi/2$, the resulting electromagnetic field is linearly polarized

$$\vec{E}(z = n\frac{\pi}{2}, t) = \sqrt{2}E_0\left[\frac{\hat{x} \pm \hat{y}}{\sqrt{2}}\cos\omega t\right]. \tag{4.35}$$

In between these points, where $kz = (2m+1)\pi/4$, the resulting electromag-

netic field

$$\vec{E}(z = (2m+1)\frac{\pi}{4}, t) = E_0 \left[\frac{\hat{x}+\hat{y}}{\sqrt{2}} \cos\omega t \pm \frac{\hat{x}-\hat{y}}{\sqrt{2}} \sin\omega t \right] \qquad (4.36)$$

displays circular polarization, whose handedness depends on the position z. This strong polarization gradient is the key to sub-Doppler cooling of multilevel atomic gases.

The regions of circular polarity are the most interesting and relevant to sub-Doppler cooling schemes. In these regions, the AC Stark effect shifts the energy levels of the ground state, where the magnitude of this shift is proportional to the electromagnetic coupling to the excited states, which is different for each sub-level in the ground-state manifold. Populations of atoms near these locations of circular polarization will be optically pumped into the lowest lying ground state. Atoms possessing a kinetic energy greater than the local ground state energy splitting can move non-adiabatically by a quarter wavelength into a region of opposite circular polarization. In traveling to this new region of higher potential energy, some of the atom's kinetic energy must have been lost. This excess potential energy escapes as a photon during the process of optical pumping, resulting in the atom's transfer to the local ground state. This effect was first described by Dalibard and Cohen-Tandouji [31], who named the process "Sisyphus cooling" from the Greek mythological figure whose punishment was to push a boulder up a hill, but whenever he completed his task, he would once again find himself at the bottom of the hill.

The theoretical lower temperature limit of Sisyphus cooling is set by the atomic recoil after a spontaneous emission, and is an order of magnitude lower than the lowest temperature achievable by Doppler cooling. In fact, this temperature is low enough that the atoms can be cooled to temperatures comparable to the ground state energy splitting! Atoms reaching this temperature will experience positional quantum effects due to the discrete energy levels in the periodic optical potential.

The experimental realization of quantum potential with perfect spatial periodicity substantially broadened the scope of the research into cold atomic gases. Many condensed matter theories were developed under the assumption of perfect periodicity, where the potential is supplied by the crystal lattice of atoms in a solid. The discrete translational symmetry plays a central role in many of the theoretical proposals,but extrinsic effects, such as dislocations, chemical impurities and surface effects, can break the translational symmetry

resulting in significant difficulty comparing theory with experiment. Cold atomic gases in optical lattices do not suffer from any of these extrinsic effects, and are a perfect candidate to study a diverse range of theoretical models.

4.3 Exploring Quantum Coherence and Correlations in Cold Atomic Gases

Coherence and correlations are reciprocal properties of quantum systems. Correlations occur when interparticle interactions are strong: Two widely separated parts of the system behave differently, but their behaviours are *dependent* upon one another[4]. Conversely, two widely separated parts of a coherent system, while *independent*, behave identically.

The main tool used in cold atom experiments is optical imaging of the gas after free expansion. This technique is particularly well suited to study quantum coherence, although it has been recently demonstrated that the images also contain information revealing the quantum correlations present in the system. We will therefore investigate this technique by examining two important experiments.

The seminal experiment that magnificently displayed coherence was that of Andrews *et. al.* [32]. They split a single sodium condensate into two by focusing a blue detuned laser onto the centre of the trap, using the dipole force to create a double well potential. Upon release, and subsequent imaging, high contrast matter-wave interference fringes were clearly seen. The theoretical explanation for these fringes, while naïvely clear, is actually quite subtle. There are a large number of papers which address this issue from the point of view that the quantum measurement process projects the many-body wavefunction into a state with a well defined relative phase *after the condensates have been released from the trapping potential.* We present here a novel calculation that takes a slightly different point of view. We investigate the resulting entangled state that results after a number of particles have leaked out of the trap, but prior to releasing the condensates from the trapping potential.

[4]The interparticle interaction does not have to be strong *at the moment the correlations are detected.* A Bell state, for instance, displays correlations even when the particles are widely separated. The correlations result from the initial state preparation, where the particles were strongly interacting.

To begin our investigation, we consider two isolated systems, both in Fock states

$$|N_1, N_2\rangle = \frac{\left(a_1^\dagger\right)^{N_1}\left(a_2^\dagger\right)^{N_2}}{\sqrt{N_1!N_2!}}|0\rangle. \tag{4.37}$$

We define the state

$$|k\rangle \equiv a^k|N_1, N_2\rangle \tag{4.38}$$

$$= 2^{-k/2}\left(a_1 + e^{i\phi}a_2\right)^k|N_1, N_2\rangle, \tag{4.39}$$

which corresponds to the state of the system 4.37 after k particles have been removed. We imagine that this removal of particles happens because the isolated Fock states "leak", and the environment observes the resulting particles, but it does not know from which subsystem each particle came. The state $|k\rangle$ is a huge superposition of all the ways k particles can be taken away from either of the two subsystems

$$|k\rangle = 2^{-k/2}\sum_{j=0}^{k}\binom{k}{j}e^{i\phi(k-j)}\sqrt{\frac{N_1!N_2!}{(N_1-j)!(N_2-k+j)!}}|N_1-j, N_2-k+j\rangle. \tag{4.40}$$

Since we are investigating Fock states being driven into a state of definite relative phase, we project the state $|k\rangle$ onto the set of "phase states"

$$|\theta_m\rangle = \frac{1}{\sqrt{s+1}}\sum_{n=0}^{s}e^{in\theta_m}|n\rangle, \tag{4.41}$$

which are *almost* the Fourier conjugate to the number states. In the full infinite dimensional Hilbert space, these states are not orthonormal – a result of the negative number states being unphysical and therefore not present in the Hilbert space. However, it is shown in [5] that restricting the Hilbert space to contain only s particles circumvents these issues. As a result, however, the phase states are discretized:

$$\theta_m = \frac{2\pi m}{s+1} \tag{4.42}$$

where m runs from 0 to s. In the truncated Hilbert space, the phase states are orthonormal, and have a resolution of the identity operator. At the end

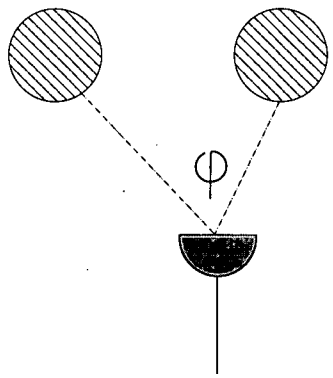

Figure 4.1: Schematic representation leading to the state $|k\rangle$ 4.39. The environment, which observes the particles coming from either BEC, is encompassed by a single detector at an arbitrary location. The phase difference ϕ is wholly due to the path difference in the free motion between the two condensates.

of the calculation, one can usually take $s \to \infty$ and recover the continuous phase variable.

Multiplication of the state $|k\rangle$ by the resolution of the identity

$$1 = \sum_{pp'=0}^{s} |\theta_p \theta_{p'}\rangle\langle\theta_p \theta_{p'}| \tag{4.43}$$

leads to the state

$$\begin{aligned} |k\rangle \;=\; & \frac{2^{-k/2}}{s+1} \sum_{pp'} \sum_{j=0}^{k} \binom{k}{j} \sqrt{\frac{N_1! N_2!}{(N_1-j)!(N_2-k+j)!}} \\ & \times e^{-i\theta_p(N_1-j) - i\theta_{p'}(N_2-k+j)} e^{i\phi(k-j)} |\theta_p \theta_{p'}\rangle. \end{aligned} \tag{4.44}$$

The state 4.44 is a completely general form for any value of the particle numbers N_1, N_2 and number of anihilations k. What we are seeking, however, is a limiting form of 4.44 when the particle numbers are large, $N_1, N_2 \gg 1$. We therefore define the function

$$f(j) = \binom{k}{j} \sqrt{\frac{N_1! N_2!}{(N_1-j)!(N_2-k+j)!}} \tag{4.45}$$

and perform an expansion about its maximum value. It turns out to be easier to expand the logarithm of 4.45, which is permissible since the logarithm is a monotonically increasing function. This procedure results in the series

$$\ln f(j) \approx \ln f(\bar{j}) - \frac{1}{2\sigma^2}(j-\bar{j})^2 \tag{4.46}$$

where $\bar{j}$ is the solution of the equation

$$\bar{j}^2\left(N_2 - k + \bar{j}\right) = (k-\bar{j})^2\left(N_1 - \bar{j}\right), \tag{4.47}$$

and

$$\frac{1}{\sigma^2} = \frac{1}{k-\bar{j}} + \frac{1}{\bar{j}} + \frac{1}{2\left(N_2 - k + \bar{j}\right)} + \frac{1}{2\left(N_1 - \bar{j}\right)}. \tag{4.48}$$

Inserting this expansion into the state 4.44 gives

$$|k\rangle = \frac{2^{-k/2}}{s+1}\sum_{pp'}\int_{-\infty}^{\infty} \mathrm{d}j\mathcal{N}e^{-\frac{1}{2\sigma^2}\left(j-\bar{j}\right)^2}e^{i\bar{j}\left(\theta_p-\theta_{p'}-\phi\right)}e^{-i\theta_p N_1 - i\theta_{p'}(N_2-k)}|\theta_p\theta_{p'}\rangle \tag{4.49}$$

which, after integration over j and normalization, gives the exactly the sought-after state

$$|k\rangle = \frac{\sqrt{2\pi^{1/2}\sigma}}{s+1}\sum_{pp'} e^{-\frac{1}{2}\left(\theta_p-\theta_{p'}-\phi\right)^2}e^{-i\theta_p\left(N_1-\bar{j}\right)}e^{-i\theta_{p'}\left(N_2-k+\bar{j}\right)}|\theta_p\theta_{p'}\rangle. \tag{4.50}$$

This represents the major result of this section, the many-body state for two separated condensates after many leaks becomes a state of totally uncertain average phase, but one whose relative phase is certain.

In the special case where $N_1 = N_2 = N$, we can go even further. The implicit equation that solves for $\bar{j}$ admits the solution $\bar{j} = \frac{k}{2}$, and the width of the Gaussian spread can be calculated exactly

$$\frac{1}{\sigma^2} = \frac{(4N-k)}{k\left(N-\frac{k}{2}\right)} \tag{4.51}$$

$$= \frac{4}{k} + \frac{1}{N} + \frac{1}{2N^2}k + \mathcal{O}\left(\frac{k}{N^3}\right). \tag{4.52}$$

This physically demonstrates that as more particles leak out of the Fock state and get observed by the environment, the spread in relative phase decreases.

In the limit where the particle numbers are almost equivalent $N_1 = N+\Delta$, and $\Delta/N \ll 1$ the average particle number $\overline{j}$ takes on the modified value

$$\overline{j} = \frac{k}{2}\left(1 + \frac{\Delta}{(4N-k)}\right) \tag{4.53}$$

and the spread becomes

$$\frac{1}{\sigma^2} = \frac{4}{k} + \left(\frac{1}{N} - \frac{\Delta}{2N^2}\right) + \left(\frac{1}{2N^2} - \frac{\Delta}{2N^3}\right)k + \mathcal{O}\left(\frac{k^2}{N^3}\right). \tag{4.54}$$

In summary, coherence is a natural consequence of experimental imperfections of the trap. Furthermore, it has been shown that the measurement process itself forces two Fock states into a state of definite relative phase [33]. This calculation proceeds in a similar fashion to the one presented here, where the measurement process collapses the wavefunction into an eigenstate of the measurement operator. When probing atomic density, the measurement operator is a large product of anihilation operators, whose eigenstates are states of definite phase. However, each experiment will see only "one-shot" of the wavefunction 4.50 – from experiment to experiment the actual relative phase will be unpredictable, and furthermore, averaging over many experimental runs will destroy this coherence.

It is important to clarify that we do not believe the calculation presented here represents the true physical mechanism that produces the sharp interference fringes seen in experiments. In fact, it has been shown that two pure Fock states will exhibit these fringes, and they arise solely due to the physical measurement process [33]. The main conclusion of this calculation is that a sharply defined phase difference between two initially isolated condensates is an inevitability, whether it arises from interaction with the environment, as suggested here, of a natural result of the act of measurement.

However, this calculation does give rise to the interesting possibility of engineering coherences by simply observing the particles that have leaked out of the traps. Measurement induced coherences have been hypothesized as a possible route to quantum computing [34]. While an intriguing possibility, this line of research will not be considered further in this thesis.

While coherence is both an interesting and intriguing property, it does not reveal physical information about the underlying system. In the previous example, it is not the interference fringes themselves, but the wavelength of these fringes that gives the physical information – in the form of a de Broglie

wavelength. Furthermore, coherence is not a robust property of the system – the same relative phase does not persist from experiment to experiment.

In order to develop a methodical process to extract physical information, the auto-correlation function

$$C(y) = \frac{\int \mathrm{d}x \langle n(x)n(x+y)\rangle}{\int \mathrm{d}x \langle n(x)\rangle\langle n(x+y)\rangle} \tag{4.55}$$

is introduced, where the angular brackets denote averaging over all experiments

$$\langle n(x)\rangle = \frac{1}{N}\sum_{i=1}^{N} n_i(x). \tag{4.56}$$

The function 4.55 is constructed to draw out the information that persists between experiments. To illustrate this method, we have constructed data sets corresponding to 200 realizations of the function

$$f_i(x) = e^{-\frac{x^2}{10}} \sin^2(x+\phi_i) \tag{4.57}$$

in figure 4.2 (where the phases ϕ_i are chosen randomly in the range $[0, 2\pi]$)[5].

The preceding example demonstrates the principle of extracting physical information by investigating persistent features from many experimental images. In order to demonstrate the true power of this technique, however, we will briefly discuss an early optical lattice experiment.

Bosonic atoms confined in an optical lattice are well described by the Hubbard model [35]

$$H = -t\sum_{\langle ij\rangle}\left\{a_i^\dagger a_j + \text{h.c.}\right\} + \frac{U}{2}\sum_i n_i(n_1 - 1). \tag{4.58}$$

This model displays a phase transition between superfluid behaviour and a strongly correlated insulating state as the ratio of the energy scales U/t is changed. The kinetic term in the Hamiltonian is dominant below the critical value $U/t < U_c = z \cdot 5.83$ (where z is the number of nearest neighbour lattice sites), resulting in superfluid behaviour where all particles are delocalized

[5]This functional form was chosen to mimic the particle density resulting from a free expansion of two isolated Bose-Einstein condensates with a definite relative phase, and a four collinear BEC's respectively.

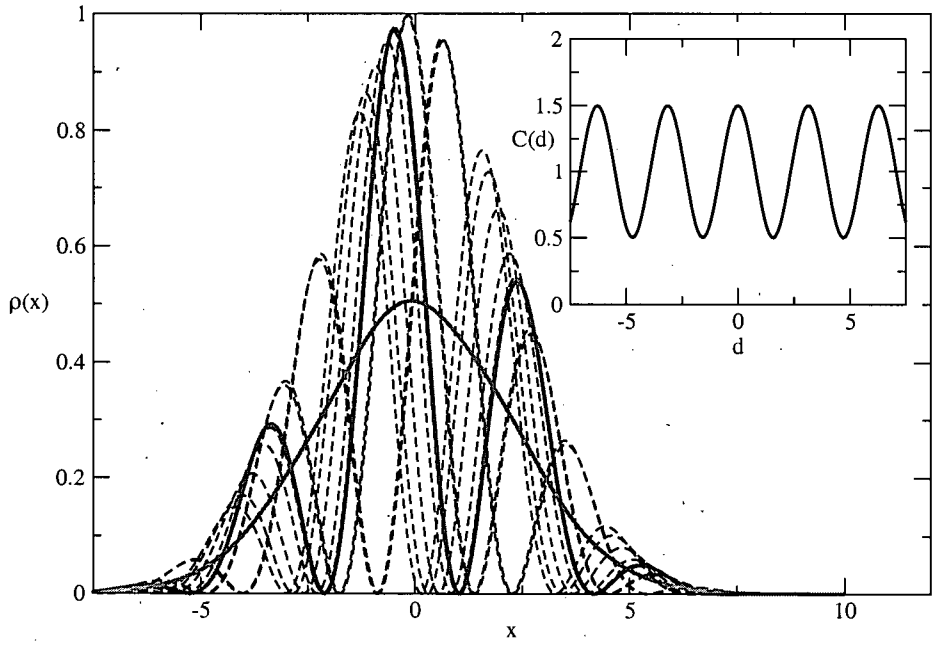

Figure 4.2: Illustrative example of auto-correlation function, equation 4.55. The broken black lines display a subset of 20 of 200 realizations of the function 4.57 with randomly chosen phases (one specific realization is highlighted with a solid blue line for clarity). The solid red line is the average over all realizations given by equation 4.56. The inset displays the auto-correlation of the data set, equation 4.55. If the data is perfectly coherent, the numerator in equation 4.55 factors, and $C(y) = 1$ for all values of y. When this function differs from one, correlations are present. The sinusoidal variation of the auto-correlation function clearly demonstrates the correlations present in this artificial data set.

throughout the lattice [36]. In the other limit $U/t > U_c$ double occupancy of any one lattice site becomes energetically unfavourable, and hopping is therefore suppressed. This leads to Mott insulating behaviour, an insulator whose properties stem from the strong correlations and not band structure considerations.

This transition was tested experimentally by loading Bosonic atoms into a three dimensional cubic lattice and changing the lattice depth by controlling the intensity of the laser light used to create the optical lattice [37]. Releasing the gas from the trapping potential and imaging it after a time of free expansion reveals striking images of the two phases.

To understand the images, we look at the particle density after a time of flight[6]

$$\langle n(x,t)\rangle = \frac{1}{W^d}\sum_{ij} e^{iQ(x)\cdot(x_i-x_j)}\langle\Psi|a_i^\dagger a_j|\Psi\rangle. \tag{4.59}$$

In the superfluid state, the system is described by the wavefunction

$$|\Psi\rangle = \left(\sum_{i=1}^{M} a_i^\dagger\right)^N |0\rangle, \tag{4.60}$$

where each of the N particles are in the ground state ($k = 0$ momentum state) of the Brillouin zone. In this state, the bilinear operator

$$\langle\Psi|a_i^\dagger a_j|\Psi\rangle = |\Psi|^2 \tag{4.61}$$

is a constant and the particle density 4.59 vanishes unless $Q(x)$ is a reciprocal lattice vector. This result is quite remarkable; the resulting particle density directly images the reciprocal lattice!

The Mott insulating state is described by the wavefunction

$$|\Psi\rangle = \prod_{i=1}^{M} a_i^\dagger|0\rangle \tag{4.62}$$

[6]This expression is derived by projecting the wavefunctions onto the lowest eigenstate of the optical potential and choosing a Gaussian basis for the Wannier orbitals. In the long time limit (analogous to the far-field approximation in optics), we can approximate the Gaussian by a width W. The momentum $Q(y) = \frac{hy}{mt}$ defines a relationship between the momentum in the trap before expansion, and the location of the particle after expansion.

where an integer number of particles are placed on each lattice site. Since double occupancy is prohibited, the bilinear operator acts as a Kronecker delta

$$\langle \Psi | a_i^\dagger a_j | \Psi \rangle = \delta_{ij}. \tag{4.63}$$

Inserting this result into the particle density 4.59 results in a "featureless" particle density after expansion. Both of these scenarios are borne out in the actual experiment [37].

It is unsatisfying that the interesting highly correlated many-body state displays no signatures of its correlations. However, inserting the Mott wavefunction 4.62 into the experimentally averaged self-correlator 4.55 reveals something interesting [38]:

$$C(y) = 1 + \frac{1}{N^2} \sum_{ij} e^{iQ(y)\cdot(x_i - x_j)}. \tag{4.64}$$

The fluctuations in the experimental signal have a signature that persists between experimental runs! The quantum correlations present in the Mott insulating state show up as reciprocal lattice peaks in the self-correlation function. Therefore, this data processing technique can reveal interesting physical information hidden in the experimental data, information that can be used to probe quantum correlations in physical systems.

The 1924 prediction of Bose-Einstein condensation resulted in a 70 year experimental search, whose culmination occurred in 1995 with the realization of a BEC composed of ultracold alkali atoms. The research into BEC's in the years following this discovery has had significant applications to a wide range of physical disciplines. With the creation of optical lattices, and a method to probe correlation physics, the future applications of BEC's in the next decade promises to be just as revolutionary.

CHAPTER 5

ENGINEERING DIRAC FERMIONS IN OPTICAL LATTICE SYSTEMS

The periodic potentials available with the application of coherent laser light on cold atomic gas systems, with *perfect* periodicity, allows for the testing of many condensed matter paradigms. In this way, the field of atomic physics can engineer systems to behave as "analogue quantum computers", in the sense that Richard Feynman originally intended when he considered the concept of computation with quantum systems in 1982 [39].

The purpose of this chapter is to propose a method of engineering cold Fermionic gases in the presence of an optical lattice into a state whose low energy excitations are Dirac Fermions described by the equation

$$(\gamma_\mu \partial_\mu - m)\psi = 0. \tag{5.1}$$

Dirac Fermions arise in many condensed matter systems [40–42], and are of simultaneous interest to high energy theory [43] where chiral symmetry breaking has been studied as an avenue to dynamical mass generation.

The advantage of studying Dirac Fermions in optical lattice systems is the high amount of control afforded by the experimental setup. Specifically, the Fermionic interaction parameters are controllable by simply changing the intensity of laser light. Therefore, a complete quantum phase diagram for interacting massless Dirac Fermions can be mapped by simply controlling the intensity of the laser light.

Cold Fermionic gases in the presence of an optical lattice are well described by the Fermionic tJU model [44, 45]

$$H = -t \sum_{\langle ij \rangle \sigma} \left(c^\dagger_{i\sigma} c_{j\sigma} + h.c. \right) + U \sum_i n_{i\uparrow} n_{i\downarrow} + J \sum_{\langle ij \rangle} \vec{S}_i \cdot \vec{S}_j \tag{5.2}$$

where the two degenerate states in the ground state manifold (the two lowest lying hyperfine states of Lithium 6, for example) have been denoted as $\{\uparrow, \downarrow\}$.

The three parameters of the model t, J and U all depend sensitively on the height of the optical lattice, which is continuously controllable by changing the intensity of laser light.

The emergence of Dirac Fermions requires both a bipartite lattice, which is a lattice that can be naturally divided into two interpenetrating sublattices, and exact particle-hole symmetry. The bipartite lattice gives rise to the spinor structure of the equations, and the permutation symmetry that exists when particles and holes can be interchanged gives rise to the symmetric nature of spatial and temporal derivatives. The combination of these two symmetries is responsible for the emergent relativistic structure of the effective Lagrangian. This can be constructed on a square lattice by threading each unit cell with exactly one half of a quantum of flux. The magnetic field changes the hopping matrix element t by the usual Peierls substitution [23], which introduces an alternating sign on every other bond. Half filling is achieved by tuning the chemical potential so there is exactly one Fermion per lattice site. This method requires the realization of an "effective magnetic field" that acts on neutral particles, which has been proposed [46, 47], but has yet to be realized experimentally.

Alternatively, the bipartite lattice can be achieved by creating a triangular lattice with a two atom basis, i.e. a honeycomb lattice. The honeycomb lattice can be experimentally achieved by six lasers with a red detuning, or by three lasers with a blue detuning. The difference lies since red detuning corresponds to trapping in the minima of the potential, so-called "low-field seeking", implying that the full honeycomb lattice would need to be implemented via six lasers. On the other hand, blue detuning corresponds to high-field seekers, and the maxima of a triangular optical lattice is a honeycomb lattice. Therefore only three lasers are required. This setup is possible in principle, and experimentally straightforward, so we concentrate on the honeycomb lattice at half filling.

The honeycomb lattice can be described by a triangular Bravais lattice with primitive vectors $\vec{a}_1 = \frac{\sqrt{3}}{2}a\hat{x} + \frac{3}{2}a\hat{y}$ and $\vec{a}_2 = \sqrt{3}a\hat{x}$ with a two-site basis described by the vector $\vec{b} = a\hat{y}$. We denote the two sub-lattices by the subscripts A and B.

To find the spectrum of the free Hamiltonian, we introduce a spinor operator whose elements are Fermionic operators that act on the two different

sub-lattices

$$d_\alpha(nm) = \begin{pmatrix} c_{A\alpha}(nm) \\ c_{B\alpha}(nm) \end{pmatrix}, \tag{5.3}$$

where $c_{A\alpha}(nm) = c_\alpha\left(\vec{R}_{nm}\right)$, $c_{B\alpha}(nm) = c_\alpha\left(\vec{R}_{nm} + \vec{b}\right)$, and $\vec{R}_{nm} = n\vec{a}_1 + m\vec{a}_2$ is the generalized triangular lattice vector. In momentum space,

$$H_0 = -t\sum_{\vec{k}\alpha} d^\dagger_\alpha(\vec{k}) \begin{pmatrix} 0 & h(\vec{k}) \\ h^*(\vec{k}) & 0 \end{pmatrix} d_\alpha(\vec{k}), \tag{5.4}$$

the energy spectrum is easily found to be

$$\epsilon = \pm|h(\vec{k})| = \pm t\sqrt{3 + 2\cos\vec{k}\cdot\vec{a}_1 + 2\cos\vec{k}\cdot\vec{a}_2 + 2\cos\vec{k}\cdot(\vec{a}_1 - \vec{a}_2)}, \tag{5.5}$$

where $h(\vec{k}) = e^{-i\vec{k}\cdot\vec{b}}\left(1 + e^{-i\vec{k}\cdot\vec{a}_1} + e^{i\vec{k}\cdot(\vec{a}_1-\vec{a}_2)}\right)$.

There has been renewed interest in this system, whose energy contour diagram is plotted in figure 5.1, because of a remarkable new technique of obtaining perfect two dimensional crystals [48]. Due to the low dimensionality, single layers of graphene sheets are predicted to display an unconventional integer quantum hall effect [49], which has recently been seen experimentally [50]. The realization of this system with an optical lattice has the advantage that the interaction is necessarily short ranged, since the atoms are neutral, and the magnitude of the interaction can be tuned continuously and a whole phase diagram is accessible in a single system.

At exactly half filling, the Fermi surface becomes a set of two points

$$\vec{k}_F^{(1,2)} = \pm\frac{4\pi}{3\sqrt{3}a}\hat{y}, \tag{5.6}$$

with the upper sign corresponding to the label 1 and the lower sign to 2. We will refer to these Fermi points as "nodes". There are four other apparent nodes in the Brillouin zone that are equivalent to $\vec{k}_F^{(1,2)}$ up to a reciprocal lattice translation $\vec{K}_{ab} = a\vec{\kappa}_1 + b\vec{\kappa}_2$, where $\vec{\kappa}_1 = \frac{4\pi}{3a}\hat{y}$ and $\vec{\kappa}_2 = \frac{2\pi}{3a}\hat{y} + \frac{2\pi}{\sqrt{3}a}\hat{x}$.

Our goal is to write an effective theory that describes the low energy Fermionic excitations, so we restrict our focus to momentum vectors in the nodal regions. Near $q = \vec{k}_F^{(1,2)}$, the off diagonal elements of the Hamiltonian density become

$$h^{(1)}(\vec{q}) = h\left(\vec{q} + \vec{k}_F^{(1)}\right) = \frac{3}{2}a\left(-q_x + iq_y\right) \tag{5.7}$$

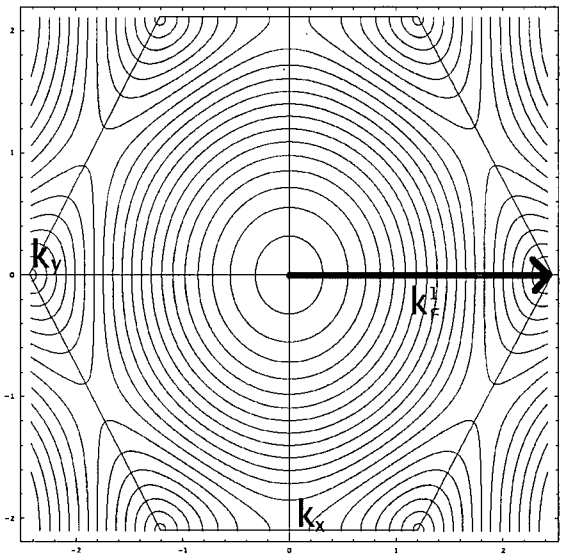

Figure 5.1: Positive solution of equation 5.5, depicting the band structure of a honeycomb lattice.

and

$$h^{(2)}(\vec{q}) = h\left(\vec{q} + \vec{k}_F^{(2)}\right) = \frac{3}{2}a\left(-q_x - iq_y\right), \tag{5.8}$$

respectively. This allows us to write the free Hamiltonian in terms of 2×2 Pauli matrices[1]

$$\begin{aligned} H_0 &= -\frac{3}{2}ta\sum_{\vec{q}\alpha}\left\{d_\alpha^{(1)\dagger}(\vec{q})\left[-\sigma_1 q_x - \sigma_2 q_y\right] d_\alpha^{(1)}(\vec{q})\right. \\ &\quad \left. + d_\alpha^{(2)\dagger}(\vec{q})\left[-\sigma_1 q_x + \sigma_2 q_y\right] d_\alpha^{(2)}(\vec{q})\right\}. \end{aligned} \tag{5.9}$$

To simplify our Hamiltonian, we introduce the velocity $c = \frac{3}{2}ta$ and the 4-spinor

$$\psi_\alpha(\vec{q}) = \begin{pmatrix} \sigma_1 d_\alpha^{(1)}(\vec{q}) \\ d_\alpha^{(2)}(\vec{q}) \end{pmatrix}, \tag{5.10}$$

[1]We use the standard basis introduced in chapter 2. In this chapter, matrices defined by $\vec{\eta}$ and $\vec{\tau}$ will also represent the 2×2 Pauli matrices in the standard basis.

whose elements create an excitation at opposite nodes. The multiplication by the σ_1 matrix serves to rotate the coordinates of the first node, so that the form of the two nodal Hamiltonians will be identical. After these transformations, the Hamiltonian becomes

$$H_0 = -c\sum_{\vec{q}\alpha} \psi^\dagger_\alpha \left[-\mathbb{1}\otimes\sigma_1 q_x + \mathbb{1}\otimes\sigma_2 q_y\right]\psi_\alpha(\vec{q}). \tag{5.11}$$

Further simplification results from defining the 4×4 Dirac gamma matrices $\gamma_\mu = \eta_3\otimes\{\sigma_3,\sigma_2,\sigma_1\}$ (where $\mu = 0,1,2$), $\gamma_3 = \eta_2\otimes\mathbb{1}$, and $\gamma_5 = \eta_1\otimes\mathbb{1}$ which satisfy the Clifford algebra $\{\gamma_\mu,\gamma_\nu\} = 2\delta_{\mu\nu}$, as well as the "relativistic" adjoint $\overline{\psi}_\alpha(q) = i\psi^\dagger_\alpha(q)\gamma_0$. The resulting Hamiltonian

$$H_0 = c\sum_{\alpha\vec{q}} \overline{\psi}_\alpha(\vec{q})\gamma_i q_i \psi_\alpha(\vec{q}) \tag{5.12}$$

represents free massless Dirac Fermions.

The general program to follow in order to investigate the interactions in this model is to convert the interacting part of the original Hamiltonian into 4-spinor notation, and to decouple the four-Fermion interactions into two-Fermion interactions by introducing an auxiliary field via the Hubbard-Stratonovich transformation[2].

We begin by investigating the Fermionic Hubbard term

$$H_U = U\sum_i n_{i\uparrow}n_{i\downarrow}, \tag{5.14}$$

we can write this Hamiltonian up to a renormalization of the chemical potential, in the form

$$H_U = -\frac{4}{3}U\sum_i \vec{S}_i^2, \tag{5.15}$$

[2]The Hubbard-Stratonovich transformation makes use of the identity

$$\sqrt{\frac{\pi}{a}}e^{\frac{b^2}{4a}} = \int \mathrm{d}x e^{-ax^2+bx} \tag{5.13}$$

to transform a Hamiltonian quartic in an operator (for example, $b = \hat{a}^\dagger\hat{a}$) into a Hamiltonian that is quadratic in that operator, at the price of introducing an auxiliary field (in this example, x). The transformation is exact when the auxiliary field is integrated over completely. It forms the basis of mean-field theory when the saddle point solution is used. For a more rigorous definition, please consult [51].

by invoking the Fierz identity $\vec{\tau}_{\alpha\beta} \cdot \vec{\tau}_{\gamma\delta} = \delta_{\alpha\delta}\delta_{\beta\gamma} - \frac{1}{2}\delta_{\alpha\beta}\delta_{\gamma\delta}$ resulting in the two-Fermion effective Hamiltonian

$$H_U^{\text{eff}} = -g_1 \sum_i \vec{M}_1(\vec{r}_i)^2 + \sum_i \vec{S}_i \cdot \vec{M}_1(\vec{r}_i), \tag{5.16}$$

where $g_1 = \frac{3}{16U}$.

In order to write the Hamiltonian 5.16 in terms of our 4-spinors, we first transform to momentum space and focus near the nodes. This gives rise to only two important values of $\vec{M}_1(q)$, near $q \approx 0$, representing intranodal scattering, and $q \approx \vec{k}_F^{(1)} - \vec{k}_F^{(2)}$, representing internodal scattering. By defining

$$m_1(\vec{q}) = M_1^z(\vec{q} \approx 0), \tag{5.17}$$

and

$$m_2(\vec{q}) = M_1^z\left(\vec{q} + \vec{k}_F^{(1)} - \vec{k}_F^{(2)}\right). \tag{5.18}$$

gives rise to the final Hamiltonian[3]

$$\begin{aligned} H_U^{\text{eff}} &= -g_1 \sum_{\vec{q}} \left\{ |m_1(\vec{q})|^2 + |m_2(\vec{q})|^2 \right\} \\ &+ \sum_{\vec{k}\vec{q}} \overline{\psi}_\alpha(\vec{k}+\vec{q}) \left\{ \gamma_0 m_2(\vec{q}) + \gamma_1\gamma_5 m_1^{'}(\vec{q}) - \gamma_1\gamma_3 m_1^{''}(\vec{q}) \right\} \tau^z_{\alpha\beta} \psi_\beta(\vec{q}). \end{aligned} \tag{5.19}$$

We have here chosen the z-axis upon which magnetization will spontaneously appear. Neglecting the other terms in the Hamiltonian will not affect the criticality of the theory, which is all that we investigate here. They will give rise to Goldstone modes that could produce interesting dynamics, but they will not qualitatively affect the spontaneous mass generation.

Turning to the nearest neighbour spin interaction

$$H_J = J \sum_{\langle ij \rangle} \vec{S}_i \cdot \vec{S}_j \tag{5.20}$$

[3]The prime and double prime denote the real and imaginary components of the field respectively. For example, we can write the complex number z as $z = z' + iz''$. This notation is used in much of the condensed matter literature.

we first recast in terms of our 2-spinors in momentum space with result

$$H_J = \frac{J}{4}\sum_{\vec{k}\vec{p}\vec{q}} h(\vec{q}) d^\dagger_\alpha(\vec{p}+\vec{q})\sigma^+ d_\beta(\vec{p}) d^\dagger_\gamma(\vec{k}-\vec{q})\sigma^- d_\delta(\vec{k})\vec{\tau}_{\alpha\beta}\cdot\vec{\tau}_{\gamma\delta}, \qquad (5.21)$$

where we have defined $\sigma^\pm = \frac{1}{2}(\mathbb{1} \pm \sigma_z)$. Again, there are two important momentum regions to consider. However, in the low energy limit, the associate phase factors imply that intranodal scattering dominates, since

$$h(\vec{q}\approx 0) \approx 3 + \mathcal{O}(q^2), \qquad (5.22)$$

and

$$h(\vec{q}+\vec{k}_F^{(1)}-\vec{k}_F^{(2)}) \approx \frac{3}{2}a\left(i\frac{\sqrt{3}}{2}-\frac{1}{2}\right)q_x - \frac{3}{2}a\left(\frac{1}{2}+i\frac{\sqrt{3}}{2}\right)q_y. \qquad (5.23)$$

Therefore, only intranodal scattering is considered, resulting in the 4-spinor form of the spin Hamiltonian

$$\begin{aligned} H_J &= -\frac{3J}{16}\sum_{\vec{k}\vec{p}\vec{q}}\Big\{\psi^\dagger_\alpha(\vec{p}+\vec{q})\psi_\beta(\vec{p})\psi^\dagger_\gamma(\vec{k}-\vec{q})\psi_\delta(\vec{k}) \\ &\quad - \overline{\psi}_\alpha(\vec{p}+\vec{q})\psi_\beta(\vec{p})\overline{\psi}_\gamma(\vec{k}-\vec{q})\psi_\delta(\vec{q})\Big\}\vec{\tau}_{\alpha\beta}\cdot\vec{\tau}_{\gamma\delta}. \qquad (5.24) \end{aligned}$$

By performing the same Hubbard-Stratonovich transformation to 5.24, we arrive at the effective spin Hamiltonian

$$\begin{aligned} H_J^{\text{eff}} = g_2\sum_{\vec{q}}\left\{|M_2^z(\vec{q})|^2 + |M_3^z(\vec{q})|^2\right\} &+ \sum_{\vec{p}\vec{q}}\Big\{\overline{\psi}_\alpha(\vec{p}+\vec{q})\tau^z_{\alpha\beta}\psi_\beta(\vec{k})M_2^z(\vec{q}) \\ &+ \overline{\psi}_\alpha(\vec{q})\gamma_0\tau^z_{\alpha\beta}\psi_\beta(\vec{q})M_3^z(\vec{q})\Big\} \qquad (5.25) \end{aligned}$$

Schematically, we can write the final form of the Hamiltonian

$$\begin{aligned} H^{\text{eff}} &= c\sum_{\vec{q}\alpha}\overline{\psi}_\alpha(\vec{q})\gamma_i q_i\psi_\alpha(\vec{q}) + \sum_{i,\vec{q}} g_i|M_i^z(\vec{q})|^2 \\ &\quad + \sum_{i,\vec{p}\vec{q}}\overline{\psi}_\alpha(\vec{p}+\vec{q})\Gamma_i\tau^z_{\alpha\beta}\psi_\beta(\vec{q})M_i^z(\vec{q}), \qquad (5.26) \end{aligned}$$

where the g_i's and Γ_i's are taken from the interaction Hamiltonians 5.16 and 5.25.

In the massless phase, we can determine how the interactions renormalize the couplings by calculating the one-loop contribution to the auxiliary field propagator

$$\mathcal{D}^{(i)}(q) = \mathcal{D}_0^{(i)}(q) + \mathcal{D}_0^{(i)}(q)\Pi^{(i)}(q)\mathcal{D}^{(i)}(q), \tag{5.27}$$

where $\Pi(q)$ is the "polarization" bubble

$$\Pi^{(i)}(q) = \sum_{k\omega} \mathrm{Tr}\left[G_0(k+q,\omega+q_0)\Gamma_i G_0(k,\omega)\Gamma_i\right]. \tag{5.28}$$

A closed form for the polarization can be found using the free propagator $G_0(q) = \frac{\gamma_\mu q_\mu}{q^2}$

$$\Pi^{(i)}(q) = \mathrm{Tr}\left[\Gamma_i\gamma_\mu\Gamma_i\gamma_\mu\right]\frac{\Lambda a}{9t\pi^2} - \frac{q}{144t^2}\mathrm{Tr}\left[\Gamma_i\gamma_\mu\Gamma_i\gamma_\nu\right]\left(\delta_{\mu\nu} + \frac{q_\mu q_\nu}{q^2}\right). \tag{5.29}$$

The net result is a reduction of the original coupling constant at low momentum

$$g_i = g_{i,0} - \left(\mathrm{Tr}\left[\Gamma_i\gamma_\mu\Gamma_i\gamma_\mu\right]\frac{\Lambda a}{9t\pi^2}\right) + \mathcal{O}(q) \tag{5.30}$$

where Λ is an ultraviolet cutoff that corresponds to the size of the Brillouin zone. Therefore, all of the couplings in the original Hamiltonian are irrelevant when the system is in the sub-critical, massless phase.

The next logical step would be to calculate the critical coupling strength for all of the different possible interactions. However, we only need consider the interaction whose critical coupling g_i^c is the lowest, since this phase will be the first reached when the experimental coupling is increased from zero. Furthermore, we know that the coupling with this property is given by the Hamiltonian

$$H_{\mathrm{Int}} = \frac{4}{3J}\sum_{\vec{q}}|M^z(\vec{q})|^2 + \sum_{\vec{k}\vec{q}}\overline{\psi}_\alpha(\vec{k}+\vec{q})\tau^z_{\alpha\beta}\psi_\beta(\vec{q})M^z(\vec{q}). \tag{5.31}$$

This fact stems from a result due to M. Reenders [52], which states that interactions with "relativistic" symmetry have lower critical couplings than non-relativistic interactions. It is shown in [52] that

$$\frac{g^c_{\mathrm{NR}} - g^c_{\mathrm{R}}}{g^c_{\mathrm{R}}} \approx 2, \tag{5.32}$$

indicating that the difference is quite large. We therefore find that the entire Hamiltonian we need investigate is much simpler

$$\begin{aligned} H &= c\sum_{\vec{q}\alpha}\overline{\psi}_\alpha(\vec{q})\gamma_i q_i\psi_\alpha(\vec{q}) + \frac{4}{3J}\sum_{\vec{q}}|M^z(\vec{q})|^2 \\ &+ \sum_{\vec{k}\vec{q}}\overline{\psi}_\alpha(\vec{k}+\vec{q})\tau^z_{\alpha\beta}\psi_\beta(\vec{q})M^z(\vec{q}). \end{aligned} \tag{5.33}$$

The critical coupling can be calculated by determining the point at which the auxiliary field

$$M^z(\vec{q}) = -\frac{3J}{8}\sum_{\vec{k}}\overline{\psi}_\alpha(\vec{k}+\vec{q})\tau^z_{\alpha\beta}\psi_\beta(\vec{q}) \tag{5.34}$$

acquires a non-zero vacuum expectation value

$$mc^2 = \langle M^z(\vec{q}\to 0)\rangle = \frac{3J}{8}\int\frac{\mathrm{d}\omega}{2\pi}\sum_k \mathrm{Tr}G_{\alpha\beta}(\vec{k},\omega)\tau^z_{\alpha\beta}. \tag{5.35}$$

When this occurs, m can be grouped into the free Hamiltonian

$$H_0 = \sum_{\vec{q}}\overline{\psi}_\alpha(\vec{q})\left[c\gamma_i q_i\delta_{\alpha\beta} + mc^2\tau^z_{\alpha\beta}\right]\psi_\beta(\vec{q}) \tag{5.36}$$

indicating that the Dirac Fermions in the critical phase acquire a mass.

The critical coupling is found by solving 5.35 with the massive propagator

$$G_{\alpha\beta}(\vec{k},\omega) = \frac{(\gamma_0\omega + c\gamma_i k_i) + mc^2\tau^z_{\alpha\beta}}{\omega^2 + c^2|\vec{k}|^2 + m^2c^4}, \tag{5.37}$$

with result

$$mc^2 = \frac{3}{\pi}\Lambda at\left[1 - 2\pi^2\frac{t}{J\Lambda a}\right] \tag{5.38}$$

Therefore, below a critical value of the nearest neighbour spin interaction parameter

$$J_c = 2\pi^2\frac{t}{\Lambda a} \tag{5.39}$$

equation 5.35 has no solution, and the low lying Fermionic excitations remain gapless. Above J_c, however, the excitations acquire a mass. In order to determine what this mass corresponds to physically, it is necessary to recast the mass in terms of the original physical creation and annihilation operators acting on the two sublattices. In terms of these original operators, the relevant term in the Hamiltonian

$$H_m = mc^2 \sum_{\vec{q}} \overline{\psi}_\alpha(\vec{q}) \tau^z_{\alpha\beta} \psi_\beta(\vec{q}) \tag{5.40}$$

becomes

$$\begin{aligned} H_m &= 2mc^2 \sum_{nm} \Big\{ c^\dagger_{A\uparrow}(nm) c_{A\uparrow}(nm) - c^\dagger_{A\downarrow}(nm) c_{A\downarrow}(nm) \\ &\quad - c^\dagger_{B\uparrow}(nm) c_{B\uparrow}(nm) + c^\dagger_{B\downarrow}(nm) c_{B\downarrow}(nm) \Big\}, \end{aligned} \tag{5.41}$$

which corresponds to preferentially populating the sub-lattices with a different species of Fermion, i.e. antiferromagnetic order.

Can this antiferromagnetic order be probed experimentally? It is shown in [53] that the experimentally averaged self-correlation function 4.55 can be written as

$$C(d) = 1 + \frac{1}{N^2} \sum_{ij} e^{iQ(d)\cdot(x_i - x_j)} - 2 \sum_{ij} e^{i\frac{md}{\hbar t}\cdot(x_i - x_j)} \langle \Psi | \vec{S}_i \cdot \vec{S}_j | \Psi \rangle \tag{5.42}$$

when there is spin order present in the optical lattice system. Therefore, the Dirac Fermions acquiring a mass is heralded by a new peak appearing in the density-density fluctuations.

Dirac Fermions appear in many physical theories in many branches of physics. In condensed matter physics, for example, they play a central role in high T_C superconductivity as well as the newly realized single graphene sheets. Both of these systems show interesting and remarkable properties, and both have low dimensionality in common.

In this chapter, we have studied a method of engineering the appearance of $2d$ Dirac quasiparticles in a system of ultracold Fermions with the application of an optical lattice. The strength of the effective interaction can be experimentally tuned in these systems by simply adjusting the intensity of the laser light used to create the optical lattice. This allows for the mapping of entire phase diagrams, and has been successfully utilized in the past to

observe quantum phase transitions [37]. We predict that, at low values of the interaction parameter, the system is completely described by massless, non-interacting Fermions with a conical spectrum. As the interaction parameter is increased, a critical point is reached where the excitation spectrum acquires a gap, corresponding to the two triangular sub-lattices being populated by different spin states. This "antiferromagnetic" gap could be easily seen by state selective optical imaging, or by the appearance of a new peak in the density fluctuation correlation function.

CHAPTER 6

CONCLUSIONS

Over the past century, quantum mechanics has proven to be the most accurate and fruitful pursuit in all of the physical sciences. The tenets of quantum mechanics form the basis of particle physics, atomic physics, condensed matter physics and chemistry. Originally developed to study physics at microscopic length scales, much effort has been devoted to extending the theory to macroscopic length scales. Two physical systems that exhibit this macroscopic quantum behaviour are studied in this thesis.

The first such system was discovered in 1911, when the Dutch physicist H. K. Onnes found that liquid mercury loses all DC electrical resistance when cooled below $4.2K$. Dubbed "superconductivity", the theoretical explanation of this effect would not be known for another 40 years – partly due to the fact that quantum mechanics was still in its infancy. In 1957, Bardeen, Cooper and Schreiffer published a paper titled "The Theory of Superconductivity" [9], where they showed that a single, macroscopic quantum order parameter was responsible for the remarkable properties of superconductivity.

The second physical system studied in this thesis evolved from an experimental search to fulfill a theoretical prediction lasting over 70 years. In 1925, Albert Einstein predicted that a collection of Bosons, sufficiently cooled, would exhibit properties whose explanation lay completely outside of anything possible in classical physics. They showed that a Bose gas will undergo a transition into a new form of matter where all of the constituent particles collapse into the same quantum ground state, and essentially act as one macroscopic quantum object. The reason this so-called "Bose-Einstein" condensate resisted an experimental verification for so long was the extraordinarily low transition temperatures predicted for the dilute gases. Two experimental groups achieved Bose-Einstein condensation independently in 1995 by cooling alkali gases to within nanoKelvin of absolute zero.

Once this feat was achieved, it was quickly realized that the lasers used to cool and trap the atomic gases could be used to manipulate the atoms into perfectly periodic arrays, whose periodicity and depth could be continuously

tuned by simply adjusting the laser parameters. This technique culminated in a magnificent realization of the "Mott-Hubbard" transition, a transition between superfluid and insulating behaviour [37].

Recently, by a technique known as sympathetic cooling, Fermionic species of alkali gases have been able to be cooled to 'degenerate'[1] temperatures. Suddenly, the field of atomic physics became extremely interesting for condensed matter theorists, since delocalized degenerate Fermions in a perfectly periodic lattice is precisely what they have been studying for a century. In true condensed matter systems, however, successful models have to be robust in the presence of disorder. True systems will contain dislocations, chemical substitutions, grain boundaries and other defects that could mask and overwhelm the intrinsic beauty of these models. Optical lattices do not suffer from any of these defects, and are therefore an ideal playground to test these beautiful ideas.

Many of the new, exciting and exotic models were developed to attack the most difficult problem facing contemporary condensed matter physics: highly correlated electron system – the most famous one being high temperature superconductors.

High temperature superconductors differ from their conventional low temperature counterparts in many ways. In the thirty years following the publication of the BCS paper, much was learned about the class of conventional superconductors, including elemental superconductors and simple compounds such as $NbSe_2$ and MgB_2. These superconductors fit the paradigm of the BCS theory and its natural extension, the Migdal-Eliashberg theory, where the normal, non-superconducting state is well described by the Fermi liquid theory, and superconductivity results from an effective attractive electron-electron interaction mediated by quantized lattice vibrations – phonons.

In the early 1980's, two physical chemists G. Bednorz and K. Mueller found a perovskite compound that became superconducting at a temperature quite above the range believed possible within the BCS paradigm. Furthermore, the normal state of these high temperature superconductors did not conform to the Fermi liquid picture, and the symmetry of the macroscopic quantum order parameter was different than from conventional supercon-

[1]This refers to the temperature below which the Maxwell-Boltzmann temperature distribution ceases to be a good approximation, that is when quantum effects become important. Degenerate Bose systems do undergo a transition into a Bose-Einstein condensate, and degenerate Fermi systems are characterized by a "Fermi sea", a sharp transition in momentum space between occupied and unoccupied energy levels.

ductors. The theoretical understanding of the mysterious high temperature superconductors still remains an unsolved problem today, some 20 years after their discovery. Perhaps one reason they have eluded a theoretical explanation is the extremely strong interparticle interactions that occur in the normal state – they fall into the class of strongly correlated electron systems.

In 2000, beautiful new data emerged from the UBC laboratory of Dr. Doug Bonn and Dr. Walter Hardy. The new data revealed electronic transport in a direction perpendicular to the direction previously studied. Two remarkable and striking features were present in the data. The first was its universal behaviour – all of the data sets fell exactly onto one universal curve when the first data point was subtracted. This strongly suggests that all of the data sets can be understood within the same framework, all governed by the same Hamiltonian[2]. The second striking feature was the similar behaviour for the two control parameters: the same non-integer power law describes both the temperature dependence and the behaviour as a function of chemical doping.

Earlier work emerging from the same UBC laboratory showed a linear depletion of the quasiparticles participating in the superconductivity as a function of both temperature and chemical doping by in-plane electronic transport measurements. The explanation of the behaviour, that normal quasiparticle excitations occur within high-T_C materials with arbitrarily low excitation energy, gave some of the first indications of the unconventional symmetry of the macroscopic order parameter. The calculation that demonstrates that an order parameter with "d-wave" symmetry perfectly accounts for this behaviour is reproduced in this thesis, using modern notation. This symmetry implies the existence of nodes (regions in momentum space with a vanishing order parameter), and it is the normal-state quasiparticles that exist in this region – the so-called "nodal quasiparticles" – that are responsible for all of the low-energy transport and thermodynamic properties of high T_C materials.

The fact that the new out-of-plane transport data shows similar behaviour as a function of both temperature and chemical doping strongly suggests that nodal quasiparticles are a central ingredient of the underlying model. Also, the new data were taken with the smallest doping values yet seen.

In this thesis, we have proposed that the quasiparticles are robust, they survive in a region surrounding the node whose area shrinks as the doping

[2]In contemporary parlance, this rules out "competing orders".

parameter is lowered. This idea, coupled with a reasonably chosen interplanar tunneling matrix element successfully explains all of the features present in the data both qualitatively and quantitatively.

Although the "mechanism" that gives rise to the superconducting properties of high T_C materials (analogous to the electron-phonon coupling in conventional superconductors) is yet unknown, it is believed to be a result of the strong interactions present in the undoped "parent" compounds. These compounds are "Mott-Hubbard" insulators, whose insulating properties stem from interelectron interactions, as opposed to the traditional band structure arguments. In is not theoretically agreed upon what state results from removing electrons from a half-filled Mott-Hubbard insulator, but it is believed that solving this question is tantamount to solving the high T_C puzzle. In this light, the main result of this thesis is to establish the nodal quasiparticles as a crucial ingredient of superconductivity in the entire superconducting dome of the high T_C phase diagram.

Superconductivity is one example of a macroscopic quantum system displaying coherence; widely separated parts of the system behave identically, but independently of each other. Furthermore, when two superconductors are brought into contact with each other, interference effects result – a hallmark of coherence. The highly correlated nature of the parent high T_C compounds give rise to this macroscopic quantum coherence.

Bose-Einstein condensates have famously displayed coherence since their observation in 1995. A heuristic calculation showing how two initially isolated condensates evolve into a state of definite relative phase through interaction with the environment is presented in this thesis. Each experimental observation of the particle density after a certain time of free expansion produces an interference pattern with a random value of the phase difference. Averaging over a large number of experimental runs results in a uniform particle density, displaying no coherence – coherence is not a robust property that survives from experiment to experiment.

However, a procedure for extracting the behaviour that does persist between experiments is explained. Investigating the experimentally averaged self-correlation function will reveal important physical information that exists in the data sets. In the case of two expanding phase-locked condensates discussed above, this procedure extracts the de Broglie wavelength of the combined system.

The usefulness of this technique is demonstrated in the Mott insulating state of a BEC in a deep optical lattice. When the particle density is imaged

after a certain time of free expansion, a noisy, but seemingly "featureless" Gaussian profile is seen. However, it turns out that there are features in the experimental noise that persist between subsequent experiments, coming from the quantum correlations that exist in the highly correlated Mott state. These quantum correlations are strikingly revealed by investigating the experimentally averaged self-correlation function [38]. This proven technique for investigating quantum correlations in optical lattice systems now makes it possible to imagine engineering optical lattice systems to act as analogue quantum computers, simulating a large class of physical theories.

One such possibility is studied in this thesis – the possibility of engineering interacting Dirac Fermions in order to investigate the exciting possibility of spontaneous mass generation by the breaking of chiral symmetry.

Dirac Fermions are interesting physical objects that arise in many physical systems, across a wide range of disciplines. Most notably, they are the quasiparticle excitations responsible for all of the low-energy transport and thermodynamic properties of high T_C superconductors. We have proposed a method to create the Dirac Fermions in an optical lattice and subsequently shown that the theory has a massless phase which becomes critical as the nearest-neighbour "spin" interaction is increased. In the critical phase, a mass gap exists that corresponds to "antiferromagnetic" order, the Fermions on nearest neighbour lattice sites have differing values for their "spin" index. Signatures of the correlations present in the massive phase should be observable in the experimentally averaged self-correlation function described earlier.

The genesis of quantum mechanics was the contradiction between the tenets of classical physics and the behaviour of objects at atomic length scales. The resolution, while at odds with "common sense", beautifully and accurately explained, and predicted, the microscopic behaviour. Today, the principles of quantum physics pervade and lay the foundation for the edifice of physical science.

There are a number of exotic systems where quantum mechanics governs the behaviour of macroscopically sized objects, a situation where quantum mechanics was not originally intended to apply. It is by studying these systems that or knowledge of quantum mechanics, and of physics in general will be broadened. The investigation of macroscopic quantum behaviour, and exploring correlations and coherences found in these systems, has led to the investigation of two complementary physical disciplines in this thesis. The continuing research into the overlap between condensed matter and ultracold

atomic physics promises to deepen our understanding of both disciplines.

BIBLIOGRAPHY

[1] D. A. Bonn. Surface impedance studies of YBCO. *Czech. J. Phys.*, 46:3195, 1996.

[2] A. R. Hosseini-Gheinani. *The Anisotropic Microwave Electrodynamics of YBCO.* PhD thesis, University of British Columbia, 2000.

[3] A. Hosseini, D. M. Broun, D. E. Sheehy, T. P. Davis, M. Franz, W. N. Hardy, Ruixing Liang, and D. A. Bonn. Survival of the d-wave superconducting state near the edge of antiferromagnetism in the cuprate phase diagram. *Physical Review Letters*, 93:107003, 2004.

[4] P. A. M. Dirac. *The Principles of Quantum Mechanics.* Oxford University Press, 1958.

[5] David T. Pegg and Stephen M. Barnett. Tutorial review quantum optical phase. *Journal of Modern Optics*, 44:225–264, 1997.

[6] Roy J. Glauber. Coherent and incoherent states of the radiation field. *Physical Review*, 131:2766, 1963.

[7] A. J. Leggett. *Bose-Einstein Condensation*, chapter 19: Broken Gauge Symmetry in a Bose Condensate, page 452. Cambridge University Press, 1995.

[8] F. London and H. London. The electromagnetic equations of the supraconductor. *Proceedings of the Royal Society of London. Series A, Mathematical and Physical Sciences*, 149:71–88, 1935.

[9] J. Bardeen, L. N. Cooper, and J. R. Schrieffer. Theory of superconductivity. *Physical Review*, 108:1175–1204, 1957.

[10] A. L. Fetter and J. D. Walecka. *Quantum Theory of Many-Paricle Systems.* McGraw-Hill, 1971.

[11] G. D. Mahan. *Many Particle Physics.* Plenum Press, 1990.

[12] W. N. Hardy, D. A. Bonn, D. C. Morgan, Riuxing Liang, and Kuan Zhang. Precision measurements of the temperature dependence of λ in $yba_2cu_3o_{6.95}$: Strong evidence for nodes in the gap function. *Physical Review Letters*, 70:3999, 1993.

[13] C. C. Tsuei and J. R. Kirtley. Pairing symmetry in cuprate superconductors. *Review of Modern Physics*, 72:969–1016, 2000.

[14] P. Anderson. *The Theory of Superconductivity in the High-T_c Cuprate Superconductors.* Princeton University Press, 1997.

[15] P. W. Anderson. The resonating valence bond state in La-2 CuO-4 and superconductivity. *Science*, 235:1196–1198, 1987.

[16] A. Paramekanti, M. Randeria, and N. Trivedi. Projected wave functions and high temperature superconductivity. *Physical Review Letters*, 87:217002, 2001.

[17] Ruixing Liang, D. A. Bonn, W. N. Hardy, and David Broun. Lower critical field and superfluid density of highly underdoped $YBa_2Cu_3O_{6+x}$ single crystals. *Physical Review Letters*, 94:117001, 2005.

[18] Ruixing Liang, D. A. Bonn, and W. N. Hardy. Growth of high quality YBCO single crystals using $BaZrO_3$ crucibles. *Physica C*, 304:105, 1998.

[19] Y. J. Uemura et al. Universal correlations between T_c and ns/m^* (carrier density over effective mass) in high-T_c cuprate superconductors. *Physical Review Letters*, 62:2317, 1989.

[20] L. B. Ioffe and A. J. Millis. d-wave superconductivity in doped Mott insulators. *Journal of Physics and Chemistry of Solids*, 63:2259–2268, 2002.

[21] B. D. Josephson. Possible new effects in superconductive tunneling. *Physics Letters*, 1:251–253, 1962.

[22] T. Xiang and J. M. Wheatley. c axis superfluid response of copper oxide superconductors. *Physical Review Letters*, 77:4632–4635, 1996.

[23] R. Peierls. Zur theorie des diamagnetismus von leitungselektronen. *Z. Phys.*, 80:763, 1933.

[24] Daniel E. Sheehy, T. P. Davis, and M. Franz. Unified theory of the ab-plane and c-axis penetration depths of underdoped cuprates. *Physical Review B*, 70:054510, 2004.

[25] T. Pereg-Barnea, P. J. Turner, et al. Absolute values of the London penetration depth in $YBa_2Cu_3O_{6+y}$ measured by zero field ESR spectroscopy on Gd doped single crystals. *Physical Review B*, 69:184513, 2004.

[26] R. J. Radtke, V. N. Kostur, and K. Levin. Theory of the c-axis penetration depth in the cuprates. *Physical Review B*, 53:R522, 1996.

[27] Franco Dalfovo, Stefano Giorgini, Lev P. Pitaevskii, and Sandro Stringari. Theory of Bose-Einstein condensation in trapped gases. *Rev. Mod. Phys.*, 71(3):463–512, Apr 1999.

[28] C. J. Pethick and H. Smith. *Bose-Einstein Condesnation in Dilute Gases.* Cambridge University Press, 2002.

[29] Franco Dalfovo, Stefano Giorgini, Lev P. Pitaevskii, and Sandro Stringari. Theory of Bose-Einstein condensation in trapped gases. *Reviews of Modern Physics*, 71:463–512, 1999.

[30] O. R. Frisch. Experimenteller nachweis des einsteininschen strahlungsruckstosses. *Z. Phys.*, 86:42, 1933.

[31] J. Dalibard and C. Cohen-Tannoudji. Laser cooling below the doppler limit by polarization gradients: simple theoretical models. *Journal of the Optical Society of America B*, 6:2023, 1989.

[32] M. R. Andrews, C. G. Townsend, H. J. Meisner, D. S. Durfee, D. M. Kurn, and W. Ketterle. Observation of interference between two Bose condensates. *Science*, 275:637, 1997.

[33] Juha Javanainen and Sung Mi Yoo. Quantum phase of a Bose-Einstein condensate with arbitrary number of atoms. *Physical Review Letters*, 76:161, 1996.

[34] Micheal A. Neilson and Isaac I. Chaung. *Quantum Computation and Quantum Information.* Cambridge University Press, 2000.

[35] D. Jaksch, C. Bruder, J. I. Cirac, C. W. Gardiner, and P. Zoller. Cold bosonic atoms in optical lattices. *Physical Review Letters*, 81:3108, 1998.

[36] K. Sheshadri, H. R. Krishnamurthy, R. Pandit, and T. V. Ramakrishnan. Superfluid and insulating phases in an interacting-Boson model: Meant-field theory and the RPA. *Europhysics Letters*, 22:257, 1993.

[37] Markus Greiner, Olaf Mandel, Tilman Esslinger, Theodor W. Hänsch, and Immanuel Bloch. Quantum phase transition from a superfluid to a Mott insulator in a gas of ultracold atoms. *Nature*, 415:39, 2002.

[38] Simon Fölling, Fabrice Gerbier, Artur Widera, Olaf Mandel, Tatjana Gericke, and Immanuel Bloch. Spatial quantum noise interferometry in expanding ultracold atom clouds. *Nature*, 434:481, 2005.

[39] R. P. Feynman. Simulating physics with computers. *International Journal of Theoretical Physics*, 21:467, 1982.

[40] M. Franz and Z. Tešanović. Quasiparticles in the vortex lattice of unconventional superconductors: Bloch waves or Landau levels? *Physical Review Letters*, 84:554–557, 2000.

[41] A. Tsvelik. Field-theory treatment of the heisenberg spin-1 chain. *Physical Review B*, 42:10499–10504, 1990.

[42] K. Farakos and N. E. Mavromatos. Hidden non-abelian gauge symmetries in doped planar antiferromagnets. *Phys. Rev. B*, 57(5):3017–3030, Feb 1998.

[43] R. Jackiw and R. Rahamaran. Vector-meson mass generation by chiral anomalies. *Physical Review Letters*, 54:1219–1221, 1985.

[44] Alexander Klein and Dieter Jaksch. Simulating the $t-J-U$ Hamiltonian with atoms in optical lattices. *arXiv.org/quant-ph/0601083*, 2006.

[45] L. M. Duan. Effective Hamiltonian for fermions in an optical lattice across Feshbach resonance. *Physical Review Letters*, 95:243202, 2005.

[46] D. Jaksch and P. Zoller. Creation of effective magnetic fields in optical lattices: the Hofstadter butterfly for cold neutral atoms. *New Journal of Physics*, 5:56, 2003.

[47] E. Mueller. Artificial electromagnetism for neutral atoms: Escher staircase and Laughlin liquids. *Physical Review A*, 70:041603, 2004.

[48] K. S. Novoselov, D. Jiang, T. Booth, V. V. Khotkevich, S. M. Morozov, and A. K. Geim. Two dimensional atomic crystals. *Proceedings of the National Academy of the Sciences*, 102:10451, 2005.

[49] V. P. Gusynin and S. G. Sharapov. Unconventional integer quantum hall effect in graphene. *Physical Review Letters*, 95:146801, 2005.

[50] K. S. Novoselov, A. K. Geim, S. V. Morozov, D. Jiang, M. I. Katsnelson, I. V. Grigorieva, S. V. Dubonos, and A. A. Firsov. Two-dimensional gas of massless dirac fermions in graphene. *Nature*, 438:197, 2005.

[51] P. M. Chaikin and T. C. Lubensky. *Principles of Condensed Matter Physics*. Cambridge University Press, 1995.

[52] M. Reenders. Néel transition, spin fluctuations, and pseudogap in underdoped cuprates by a lorentz invariant four-fermion model in 2+1 dimensions. *Physical Review B*, 66:024501, 2002.

[53] E. Altman, E. Demler, and M. Lukin. Probing many-body states of ultracold atoms via noise correlations. *Physical Review A*, 70:013603, 2004.

Appendix A

Minimal Substitution in Second Quantization

The purpose of this appendix is to find the prescription one must follow to introduce the vector potential into a Hamiltonian in second quantized form by minimal substitution. A somewhat general Hamiltonian has the form

$$\hat{H}(\hat{p},\hat{r}) = \epsilon(\hat{p}) + V(\hat{r}), \tag{A.1}$$

which we will now use to find the second quantized form[1]

$$\begin{aligned}
H &= \int \frac{\mathrm{d}k\mathrm{d}k'}{(2\pi)^2}|k\rangle\langle k|\hat{H}(\hat{p},\hat{r})|k'\rangle\langle k'|. && \text{(A.2)}\\
\langle k|\hat{H}(\hat{p},\hat{r})|k'\rangle &= \langle k|\epsilon(\hat{p})|k'\rangle + \langle k|V(\hat{r})|k'\rangle && \text{(A.3)}\\
&= \epsilon(k)2\pi\delta(k-k') + \int \mathrm{d}r\mathrm{d}r'\langle k|r\rangle\langle r|V(\hat{r})|r'\rangle\langle r'|k'\rangle && \text{(A.4)}\\
&= \epsilon(k)2\pi\delta(k-k') + \int \mathrm{d}r\mathrm{d}r' e^{-ikr}V(r)\delta(r-r')e^{ik'r'} && \text{(A.5)}\\
&= \epsilon(k)2\pi\delta(k-k') + \int \mathrm{d}r e^{ir(k-k')}V(r) && \text{(A.6)}\\
&= \epsilon(k)2\pi\delta(k-k') + V(k-k') && \text{(A.7)}
\end{aligned}$$

which implies

$$H = \int \frac{\mathrm{d}k}{2\pi}\epsilon(k)|k\rangle\langle k| + \int \frac{\mathrm{d}k\mathrm{d}k'}{(2\pi)^2}V(k-k')|k\rangle\langle k'| \tag{A.8}$$

as usual. Minimal substitution is the replacement of the momentum by the canonical momentum, which generally includes the vector potential. There-

[1] While the derivation in this appendix is one-dimensional, the result holds in arbitrary dimensions by changing the integration measure from $\frac{\mathrm{d}k}{2\pi}$ to $\frac{\mathrm{d}^d k}{(2\pi)^d}$.

fore

$$\hat{H}_A = \epsilon\left(\hat{p} - eA(\hat{r})\right) + V(\hat{r}) \tag{A.9}$$

$$= \epsilon(\hat{p}) - e\frac{\partial\epsilon}{\partial\hat{p}}A(\hat{r}) + \frac{e^2}{2}\frac{\partial^2\epsilon}{\partial\hat{p}^2}A^2(\hat{r}) + V(\hat{r}) \tag{A.10}$$

The second quantized form of the Hamiltonian after the minimal substitution will have two new non-diagonal terms. The term to first order in $A(r)$ is

$$\int \frac{\mathrm{d}k\mathrm{d}k'}{(2\pi)^2}|k\rangle\langle k|A(\hat{r})|k'\rangle\langle k'| = \int \frac{\mathrm{d}k\mathrm{d}k'}{(2\pi)^2}\mathrm{d}r\mathrm{d}r'|k\rangle\langle k|r\rangle\langle r|A(\hat{r})|r'\rangle\langle r'|k'\rangle\langle k'| \tag{A.11}$$

that we can transform by first noting that a function of one variable

$$\langle r|A(\hat{r})|r'\rangle = \delta(r - r')A(r) \tag{A.12}$$

and the fact that $\langle k|r\rangle = \frac{1}{\sqrt{2\pi}}e^{ikr}$ turns the integral into a Fourier transform in the variable $(k - k')$

$$\int \frac{\mathrm{d}k\mathrm{d}k'}{(2\pi)^2}|k\rangle\langle k|A(\hat{r})|k'\rangle\langle k'| = \int \frac{\mathrm{d}k\mathrm{d}k'}{(2\pi)^2}|k\rangle\langle k'|\int \mathrm{d}r e^{ir(k-k')}A(r) \tag{A.13}$$

$$= \int \frac{\mathrm{d}k\mathrm{d}k'}{(2\pi)^2}|k\rangle\langle k'|A(k - k') \tag{A.14}$$

$$= \int \frac{\mathrm{d}k\mathrm{d}q}{(2\pi)^2}|k + q\rangle\langle k|A(k + q). \tag{A.15}$$

The second term can be dealt with in a similar manner, and the result is another integration over momentum

$$\int \frac{\mathrm{d}k\mathrm{d}k'}{(2\pi)^2}|k\rangle\langle k|A^2(\hat{r})|k'\rangle\langle k'| = \int \frac{\mathrm{d}k\mathrm{d}q\mathrm{d}p}{(2\pi)^3}|k + p + q\rangle\langle k|A(p)A(q). \tag{A.16}$$

We can now read off the second quantized Hamiltonian obtained with the minimal substitition

$$H_A = \int \frac{\mathrm{d}k}{2\pi}c_k^\dagger c_k\epsilon(k) + \int \frac{\mathrm{d}k\mathrm{d}q}{(2\pi)^2}c_{k+q}^\dagger c_k V(q)$$
$$-e\int \frac{\mathrm{d}k\mathrm{d}q}{(2\pi)^2}c_{k+q}^\dagger c_k A(q)$$
$$+\frac{e^2}{2}\int \frac{\mathrm{d}k\mathrm{d}q\mathrm{d}p}{(2\pi)^3}c_{k+p+q}^\dagger c_k A(p)A(q), \tag{A.17}$$

which represents the result of this Appendix.

Appendix B

System of Units

B.0.1 CGS-Gaussian Units

The international standard of units is the MKS system, where length is measured in metres, mass in kilograms and time in seconds. Within this system, constants of proportionality must perpetually be created and empirically determined. For example, a new unit was created for electric charge, the Coulomb. Therefore a new constant of proportionality, known as the permittivity of free space, was needed to convert Coulombs to Newtons in the force equation

$$\vec{F} = -\frac{1}{4\pi\epsilon_0}\frac{e^2}{r}\hat{r}. \tag{B.1}$$

In a seemingly different field of physics, the Biot-Savart law relates currents to magnetic fields, with another constant of proportionality, the permeability of free space

$$d\vec{B} = \frac{\mu_0 I d\vec{l} \times \hat{r}}{4\pi r^2}. \tag{B.2}$$

In a great synthesis of physics, James Clerk Maxwell completed the set of equations that unified the electric and magnetic fields. In this set of equations, one can show that the mutual interactions between the electric field and the magnetic field give rise to the wave equation, whose characteristic velocity is given by

$$v = \frac{1}{\sqrt{\epsilon_0\mu_0}}. \tag{B.3}$$

Two incredible facts emerged. First, the speed derived by Maxwell's equations is not Galilean invariant, it does not depend on the speed of the observer. And secondly, the empirically determined speed was the speed of light $c = 2.99792458 \times 10^{10}\text{cm} \cdot \text{s}^{-1}$! This inspired Einstein to develop the

special theory of relativity, in which the electric and magnetic fields are seen to be manifestations of the same phenomena. Light is an electromagnetic wave, whose speed is constant in every frame of reference.

This fact tells us that there are not really two degrees of freedom associated with electrical phenomena and magnetic phenomena. We should therefore measure the electric field and the magnetic field in the same units. This is done in the CGS-Gaussian units. The three fundamental dimensions are still length, mass and time, but they are now measured in centimetres, grams and seconds. The conceptual difference between the MKS and CGS system of units is the fact that *every other unit is a derived unit.* For example, Coulombs law is written

$$\vec{F} = -\frac{e^2}{r^2}\hat{r}, \tag{B.4}$$

which defines the dimensions of charge to be

$$\begin{aligned} [e] &= [F]^{\frac{1}{2}}[r] && \text{(B.5)} \\ &= m^{\frac{1}{2}} \cdot l^{\frac{3}{2}} \cdot t^{-1}. && \text{(B.6)} \end{aligned}$$

The unit is "stat-coulomb", or "esu", defined as the amount of charge that generates one dyne of force (10^{-5} Newtons) at a distance of one centimetre. The dimensions of the electric field are deduced from

$$\vec{F} = q\vec{E} \tag{B.7}$$

to be

$$\begin{aligned} [E] &= [F][e]^{-1} && \text{(B.8)} \\ &= m^{\frac{1}{2}} \cdot l^{-\frac{1}{2}} \cdot t^{-1}. && \text{(B.9)} \end{aligned}$$

The Lorentz force law tells us the force generated by a magnetic field

$$\vec{F} \propto q\vec{v} \times \vec{B}. \tag{B.10}$$

The constant of proportionality is set by the criteria that we measure electric and magnetic fields in the same units. To make the equality then, we must divide by c. The force due to an electromagnetic field becomes

$$\vec{F} = q\left\{\vec{E} + \frac{\vec{v}}{c} \times \vec{B}\right\}. \tag{B.11}$$

B.0.2 Natural Units

The special theory of relativity tells us that space and time are related by a set of transformations, the Lorentz transformations, that essentially "rotate" space into time and vice versa. Since space and time are not measured in the same units, there needs to be a conversion factor to relate the two. As discussed in section B.0.1 c, the speed of light, is a natural candidate for the necessary conversion.

Classical mechanics also teaches us that systems are described by a set of generalized coordinates, whose description are equivalent as long as the canonical Poisson brackets are obeyed. This means that momenta and position can be essentially "rotated" into each other by "canonical transformations", which are transformations that preserve the canonical Poisson brackets. We therefore seek a constant of proportionality that relates any two canonically conjugate coordinates. This constant must have the dimensions of action.

The next twentieth century revolution in physics introduced such a fundamental constant. Max Planck introduced a constant in order to fix the "ultraviolet" catastrophe that plagued classical physics. This constant was empirically found to have the value $\hbar = 1.05457266 \times 10^{-27}\mathrm{g} \cdot \mathrm{cm}^2 \cdot \mathrm{s}^{-1}$.

We see that twentieth century physics has given us the basis for a "natural" system of units that uses the three fundamental units of speed, action and energy as the basis, compared with mass, length and time. Action is measured in multiples of $\hbar$, speeds in fractions of c and energy in electron Volts (eV). The unit of energy is arbitrary, but once chosen, we can measure every other quantity in the units of energy.

Given a quantity in CGS X with some dimensions

$$[X] = m^a \cdot l^b \cdot t^c \tag{B.12}$$

can be converted to natural units

$$[X] = E^\alpha \cdot \hbar^\beta \cdot c^\gamma \tag{B.13}$$

via

$$\alpha = a - b - c \tag{B.14}$$
$$\beta = b + c \tag{B.15}$$
$$\gamma = b - 2a \tag{B.16}$$

and some dimensionful conversion factors

$$eV = 1.60217733 \times 10^{-12}\mathrm{g}\cdot\mathrm{cm}^2\cdot\mathrm{s}^{-2} \quad \text{(B.17)}$$
$$c = 2.99792458 \times 10^{10}\mathrm{cm}\cdot\mathrm{s}^{-1} \quad \text{(B.18)}$$
$$e = 4.80287 \times 10^{-10}\mathrm{g}^{\frac{1}{2}}\cdot\mathrm{cm}^{\frac{3}{2}}\cdot\mathrm{s}^{-1} \quad \text{(B.19)}$$
$$\hbar = 1.05457266 \times 10^{-27}\mathrm{g}\cdot\mathrm{cm}^{-2}\cdot\mathrm{s}^{-1} \quad \text{(B.20)}$$
$$= 6.582122 \times 10^{-16}\mathrm{eV}\cdot\mathrm{s} \quad \text{(B.21)}$$
$$\hbar c = 1.97327053 \times 10^{-7}\mathrm{eV}\cdot\mathrm{cm} \quad \text{(B.22)}$$

For example

$$[\text{mass}] = \mathrm{eV}\cdot c^{-2} \quad \text{(B.23)}$$
$$[\text{length}] = \mathrm{eV}^{-1}\cdot\hbar\cdot c \quad \text{(B.24)}$$
$$[\text{time}] = \mathrm{eV}^{-1}\hbar \quad \text{(B.25)}$$
$$[\text{charge}] = \hbar^{\frac{1}{2}}\cdot c^{\frac{1}{2}} \quad \text{(B.26)}$$
$$[\text{momentum}] = \mathrm{eV}\cdot c^{-1}. \quad \text{(B.27)}$$

In natural units, the quantity $\frac{e^2}{\hbar c}$ is dimensionless, and takes the value

$$\frac{e^2}{\hbar c} \simeq \frac{(4.803)^2}{1.05457 \times 2.9979} \times 10^{-3} \quad \text{(B.28)}$$
$$\simeq 0.00729 \quad \text{(B.29)}$$
$$\simeq \frac{1}{137}. \quad \text{(B.30)}$$

Other dimensionful quantities can be readily derived just from these natural scales of nature. For example, the combination $\frac{e^2}{\hbar}$ has the dimensions of speed. It is the characteristic speed of a non-relativistic electron in a hydrogen atom and can be conveniently written $v_e = \alpha c$. The combination of constants that has the dimensions of energy (besides the rest mass of the electron) is $E_0 = m_e v_e^2 = m_e c^2 \alpha^2$. The binding energy of the electron inside a hydrogen atom is calculated to be $E_b = -\frac{1}{2}E_0$. The length scale is given by $l_e = \frac{\hbar c}{E_0} = \frac{\hbar^2}{m_e c^2}$ which is equal to the Bohr radius of the electron, denoted a_0. Another length scale can be found by dividing this number by α, and its name is the "Compton" wavelength $\lambda_c = \frac{a_0}{\alpha} = \frac{\hbar}{m_e c}$. This is the minimal De Broglie wavelength the electron can achieve, and it is that natural unit of length that arises in the Compton scattering of electrons. Finally, one

can construct a number with the dimensions of magnetic field times length squared, which is known as magnetic flux. From dimensional analysis, one sees that the CGS unit of electric charge already has this unit, however one does not expect quantization of magnetic field in terms of the electric charge alone, since the electromagnetic effects due to particle motion will scale with $\frac{v}{c}$ and Planck's constant does not appear in this formula. Therefore we take the combination $\Phi = \frac{e}{\alpha} = \frac{\hbar c}{e}$. It turns out that the quantum of flux is $\Phi_0 = 2\pi\Phi = \frac{hc}{e}$, and has the magnitude

$$\Phi_0 = 4.13375685 \times 10^{-7} \text{Gauss} \cdot \text{cm}^2. \tag{B.31}$$